A behavior-oriented dynamic model for sandbar migration and 2DH evolution

Kristen D. Splinter,[1,2] Robert A. Holman,[1] and Nathaniel G. Plant[3]

Received 29 April 2010; revised 22 October 2010; accepted 12 November 2010; published 29 January 2011.

[1] A nonlinear model is developed to study the time-dependent relationship between the alongshore variability of a sandbar, $a(t)$, and alongshore-averaged sandbar position, $x_c(t)$. Sediment transport equations are derived from energetics-based formulations. A link between this continuous physical representation and a parametric form describing the migration of sandbars of constant shape is established through a simple transformation of variables. The model is driven by offshore wave conditions. The parametric equations are dynamically coupled such that changes in one term (i.e., x_c) drive changes in the other (i.e., $a(t)$). The model is tested on 566 days of data from Palm Beach, New South Wales, Australia. Using weighted nonlinear least squares to estimate best fit model coefficients, the model explained 49% and 41% of the variance in measured x_c and $a(t)$, respectively. Comparisons against a 1-D horizontal (1DH) version of the model showed significant improvements when the 2DH terms were included (1DH and 2DH Brier skill scores were −0.12 and 0.42, respectively). Onshore bar migration was not predicted in the 1DH model, while the 2DH model correctly predicted onshore migration in the presence of 2DH morphology and allowed the bar to remain closer to shore for a given amount of breaking, providing an important hysteresis to the system. The model is consistent with observations that active bar migration occurs under breaking waves with onshore migration occurring at timescales of days to weeks and increasing 2DH morphology, while offshore migration occurs rapidly under high waves and coincides with a reduction in 2DH morphology.

Citation: Splinter, K. D., R. A. Holman, and N. G. Plant (2011), A behavior-oriented dynamic model for sandbar migration and 2DH evolution, *J. Geophys. Res.*, *116*, C01020, doi:10.1029/2010JC006382.

1. Introduction

[2] Nearshore bathymetry is highly dynamic in both space and time. While some beaches exhibit a monotonic cross-shore structure, for many the dominant offshore features are sandbars [e.g., *Lippmann and Holman*, 1989; *Ruessink et al.*, 2003]; shallow anomalies whose movement dominates bathymetric variability. Because waves can dissipate their energy over offshore sandbars away from the shoreline, sandbars act as natural coastal protection and understanding their dynamics is important to understanding coastal resiliency. Observations show the morphology of these sandbars can rarely be considered alongshore uniform over the length scales of $O(10–10^3)$ m and timescales of days to months. *Lippmann and Holman* [1990] found that sandbar morphology at Duck, North Carolina, was visibly alongshore uniform for less than 7% of a 2 year data set of daily measurements. Several studies [*Wright et al.*, 1987; *Lippmann and Holman*, 1990; *Ranasinghe et al.*, 2004] have shown that the two most commonly occurring beach states at intermediate beaches such as Duck, North Carolina, and a number of beaches in southeastern Australia are the Transverse Bar Rip and the Rhythmic Bar and Beach, accounting for 70%–80% of the temporal variation. Therefore, a full description of water depth, $h(x, y, t)$, requires specification of the cross-shore, x, alongshore, y, and temporal, t, dependencies. If we consider typical surf zone widths to range from 200 to 500 m and alongshore scales of interest between 500 and 2000 m, the number of data points required to model these domains necessitates bathymetric measurements of $O(10^3–10^6)$ depending on desired accuracy.

[3] Several approaches have been used to reduce the dimensionality of the problem. Models can be formulated to represent either 1-D horizontal (1DH), both the alongshore and cross-shore (2DH), or all three, including the depth variation (3D). Bathymetry can be represented as either a continuous variable (sampled at discrete points) or as parametric functions that are assumed to adequately represent the bulk of the continuous profile variability with a few parameters such as the location, amplitude, and length of sandbars. Each approach offers different trade-offs between simplicity and realism.

[1] College of Oceanic and Atmospheric Sciences, Oregon State University, Corvallis, Oregon, USA.
[2] Now at Griffith Centre for Coastal Management, Griffith University, Southport, Queensland, Australia.
[3] U.S. Geological Survey, Florida Integrated Science Center, St. Petersburg, Florida, USA.

0148-0227/11/2010JC006382

1.1. The 1DH Models

[4] A number of process-based models of cross-shore transport have been proposed in the literature and applied to the problem of predicting sandbar migration. Many are based on an energetics approach [e.g., *Bagnold*, 1963] that assume cross-shore processes such as undertow and velocity skewness dominate the forcing terms [e.g., *Bailard*, 1981]. Likewise, these models assume alongshore variability in the bathymetry and dynamics has a negligible impact on cross-shore sandbar migration. Beach change is modeled as a continuous function of cross-shore location, where a sandbar may be defined qualitatively as some perturbation in the mean profile. Results are often described in morphologic terms, where a judgment that a sandbar moved onshore or offshore is based on depth changes between two consecutive profiles and the identification of the bar "crest". Offshore migration is usually well predicted by energetics-based models, when feedbacks between the offshore directed mean flows (undertow) and the sandbar dominate the response [e.g., *Gallagher et al.*, 1998]. However, these models historically have failed to accurately predict the proper rates of onshore sandbar migration when mean flows are weak and wave driven processes should dominate. Observations by *Elgar et al.* [2001] during the Duck94 field experiment noted that wave acceleration skewness was strongest over the sandbar and that this could cause sand to be picked up as the steep wave face passed and then transported onshore by the wave during mild wave conditions. The model of *Hoefel and Elgar* [2003] applied an acceleration skewness-based term to the *Bailard* [1981] energetics model and were able to reproduce an onshore migration event. *Henderson et al.* [2004] used the same data set, but a 1DH wave-resolving eddy-diffusive model to show that wave-generated momentum fluxes and Stokes drift in the boundary layer could also result in onshore transport under mild wave conditions. *Ruessink et al.* [2007] recently developed another model to examine sandbar behavior and found that under mildly to nonbreaking wave conditions, near bed wave skewness and bed load transport were responsible for onshore directed transport when bathymetry was fairly alongshore uniform. These models have shown improved skill over the original energetics model under certain circumstances, but attribute onshore transport to different mechanisms suggesting the problem is not solved despite the increasing complexity of the resolved processes.

[5] Alternatively, parametric models assume that morphology can be represented using a discrete set of parameters, such as sandbar position, whose variation with time can be directly modeled without the need for explicit prediction of spatially continuous sediment transport. Model equations are generally behavioral; distillations of known physics to a few essential elements that are assumed to dominate response. One well-known example is the breakpoint model [e.g., *Roelvink and Stive*, 1989] that suggests that sandbars exist at the location of initial wave breaking due to unspecified convergences in sediment transport. Since this model is based on an equilibrium response of the bar to a particular fluid forcing, it is strictly valid when bar response is much more rapid than the rate of change of wave conditions (i.e., storms). Attempts to predict the time-varying location of bars under either instantaneous wave forcing or some time-average wave height have not been successful [*Sallenger and Howd*, 1989].

[6] *Plant et al.* [1999] recognized the need to add a dynamic aspect to the breakpoint concept, modeling not the actual alongshore-averaged bar crest position, x_c, but instead its rate of change, $\dot{x}_c$:

$$\dot{x}_c = -\tau(t)\left[x_c - x_{eq}(t)\right], \tag{1}$$

where τ^{-1} is the wave-height-dependent response time and x_{eq} is the time varying equilibrium sandbar position based on a breakpoint hypothesis:

$$x_{eq}(t) = \xi_2 H_{\mathrm{RMS},o}(t). \tag{2}$$

$H_{\mathrm{RMS},o}$ is the offshore root mean square wave height. By fitting to an extensive data set, they found that τ was well modeled as

$$\tau(t) = \xi_1 H^3_{\mathrm{RMS},o}(t), \tag{3}$$

where ξ_1 and ξ_2 are free model parameters calibrated using observations. The model was capable of reproducing the interannual sandbar behavior and as a result of the wave height dependency, response was faster during storms and the mean bar position was weighted toward the position associated with the large waves, offshore of the mean breakpoint [*Plant et al.*, 1999].

[7] Recently, *Pape et al.* [2007, 2010a] extensively tested a series of linear and nonlinear parametric (including the *Plant et al.* [1999] model) and neural network models to examine sandbar behavior. Through extensive calibration and data training, they too found good agreement between their models and the interannual cycles of bar behavior at several sites, however, shorter-scale onshore bar migrations were not consistently well modeled. They found nonlinear models outperformed similar linear models when the data did not include long-term trends, such as offshore migrating sandbars. As well, they found the system contained some degree of hysteresis and prior knowledge of sandbar location increased the model accuracy.

1.2. The 2DH Models

[8] Although several small data sets have shown that under prolonged low or oblique waves bathymetry is relatively 1DH [*Ruessink et al.*, 2001; *Feddersen and Guza*, 2003], the assumption of alongshore uniformity is not commonly valid [e.g., *Lippmann and Holman*, 1990], especially during periods of onshore bar migration. *Feddersen and Guza* [2003] observed that when the bathymetry was alongshore variable (close to shore), the measured currents were also detectably nonuniform. For periods of nonstorm conditions (down-state transitions) changes in morphology were found to follow a defined sequence [*Wright and Short*, 1984] and be more dependent on antecedent wave conditions and the preexisting morphology rather than on the instantaneous wave conditions [*Wright et al.*, 1985], suggesting morphological feedbacks influence the time-varying response of sandbars.

[9] Recent work by *Reniers et al.* [2004] and *Drønen and Deigaard* [2007] have shown that alongshore variable forcing or bathymetry drove 2DH circulation patterns and

moved sediment in such a way that growing 2DH morphology reinforced the alongshore variability in the forcing and nonlinear feedbacks governed the response. The models were capable of reproducing the bulk characteristics of 2DH systems (i.e., growing 2DH morphology in the presence of alongshore variable forcing), however, comparisons against measured bathymetric change (i.e., exact location and magnitude of developing bathymetry) showed that prediction skill rapidly degraded with time. The models were also unable to reset the system back to an alongshore-uniform bar under storm conditions. For this reason, and the general lack of temporal and spatial input bathymetry data of sufficient resolution, tests have been limited to a few field experiments.

[10] *Plant et al.* [2006] proposed an alternate, parametric approach to examine the dynamic relationship between alongshore variable morphology, $a(t)$ and sandbar position, x_c:

$$\begin{bmatrix} \dot{x}_c \\ \dot{a} \end{bmatrix} = A \begin{bmatrix} x_c \\ a \end{bmatrix} + B \begin{bmatrix} 1 \\ H^2_{\mathrm{RMS},o} \end{bmatrix}, \tag{4}$$

where A and B are coefficient matrices determined using linear regression to the data and (over dot) represents a time derivative.

[11] *Plant et al.* [2006] defined $a(t)$ as the alongshore standard deviation of bar position for all alongshore length scales between 200 and 1000 m. For a 2 month data set covering a single offshore-onshore migration cycle, they found significant links between the two terms, suggesting that knowledge of 2DH processes was required to correctly predict onshore migration rates and that bar position was required to predict alongshore variability. Although the model highlighted some interesting links, the governing equations were behavioral and lacked a sediment transport basis. The linearized formulation was only valid for small perturbations about a mean and only applicable to short records (i.e., 2 months) and allowed bar movement even in the absence of wave forcing and lacked the clear response time characterization of *Plant et al.* [1999]. A unique least squares solution required that the bar variables and the forcing varied on different timescales. When the model was tested on the data set presented in section 3, bar position and alongshore variability sometimes varied on the same timescales of the wave forcing and the influence of 2DH variability on bar migration was masked due to the inability to separate forced and self-organized (dependent on $a(t)$) physics [*Splinter*, 2009].

[12] Here we extend the work of *Plant et al.* [1999, 2006] to study the nonlinear feedbacks between 2DH morphology and sandbar position. We develop a set of dynamically coupled equations (expressed in terms of time derivatives) that are based on the principles of sediment transport. The model does not attempt to make predictions about the nature of 2DH morphology, such as the location or number of rip channels present, or the alongshore length scale of these features, but rather about the general influence of 2DH morphology on net sandbar migration rates. Specifically, we test the hypothesis that under certain wave conditions, the presence of 2DH morphology (and by proxy 2DH currents) influences the temporal variability of the alongshore-averaged sandbar position (i.e., $\dot{x}_c = f(a, x_c,$ wave forcing)).

[13] The paper is broken down as follows. In section 2 we describe the proposed model. Section 3 describes the field site and data extraction from video time exposure images. In section 4 we test the model and present results for several data sets. Our main conclusions are discussed and summarized in sections 5 and 6, respectively.

2. Theory

[14] Our goal is to develop a parametric model for sandbar migration that can be tested using commonly available remote sensing data and that has been derived sensibly from energetics-based models of sediment transport [*Bagnold*, 1963; *Bowen*, 1980; *Bailard*, 1981] (hereafter referred to as BBB). We first develop the equations in 1DH, looking at deviations about an equilibrium balance associated with changes in mean flows and the fraction of breaking waves, b. Extensions to 2DH are based on observations and assumptions about the role of 2DH processes in net cross-shore transport. The transformation from continuous to parametric variables is based on the assumption that sediment transport mainly results in bar migration rather than changing bar shape. Unless needed for clarity, the explicit spatial and temporal dependencies of variables will be dropped for convenience for the remainder of the paper. A table of symbols, dependencies, and a brief description of each is given at the end of the paper.

2.1. Fraction of Breaking *b*

[15] Observations of time exposure imagery of breaking patterns associated with sandbars show minimal change in cross-shore position in the absence of breaking, suggesting the majority of sediment transport related to active migration is dependent on breaker driven processes. The fraction of wave breaking depends on the relative wave height, $\gamma_b = H_b/h_{x_c}$, where H_b is the depth-limited breaking wave height and h_{x_c} is the depth at the bar crest:

$$h_{x_c} = x_c(\beta - \Delta_o/x_o), \tag{5}$$

where β is the mean beach slope and Δ_o/x_o is the coefficient term of a linearly increasing bar height. Note that in contrast to normal usage, γ_b in our model is a mixed variable that compares the wave height at one location (the break point) to the depth at another location (the bar crest).

[16] Based on observations from the Duck94 experiment and Nearshore Sediment Transport Study (NSTS) data (Figure 1), the fraction of breaking is parameterized using a sigmoid curve:

$$b = \frac{1}{1 + e^{\frac{-(\gamma_b - \gamma_o)}{\Gamma}}}. \tag{6}$$

The values of $\gamma_o = 0.39$ and $\Gamma = 0.055$ were chosen to best fit available data with the assumption that the measured local relative wave height (H_{RMS}/h) can be replaced with γ_b (Figure 1).

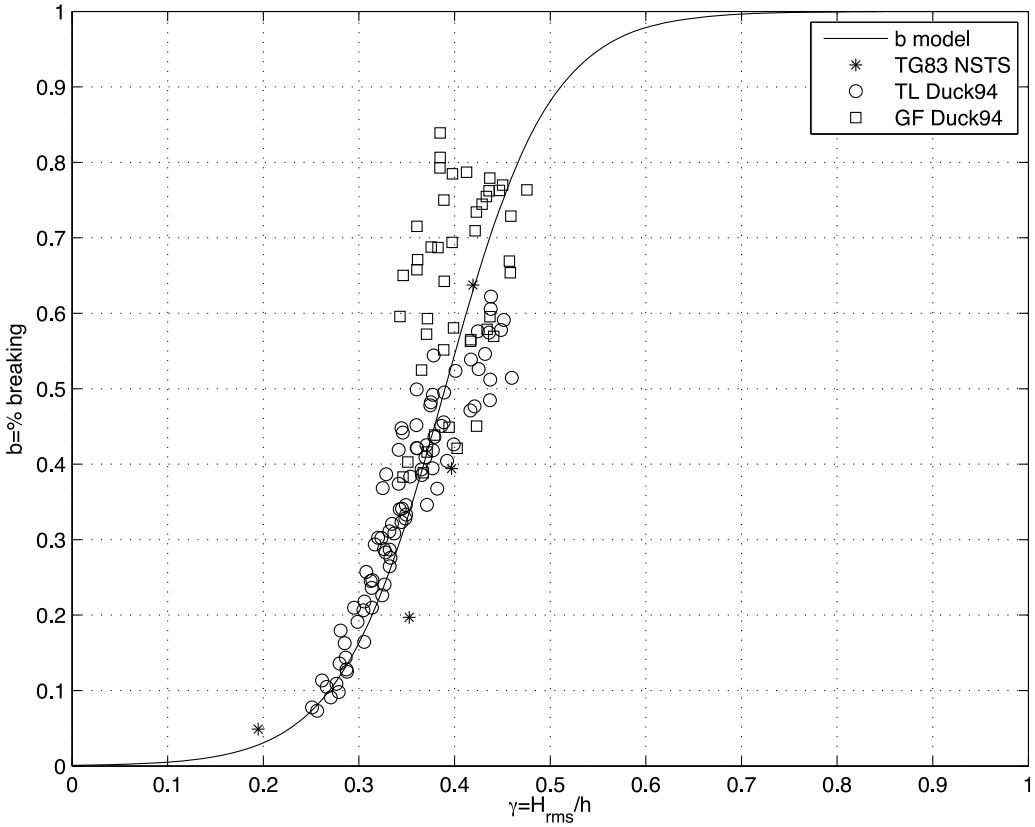

Figure 1. Percent breaking curve, b (solid line), as a function of relative wave height, H_{RMS}/h, measured across the surf zone. NSTS data digitized from *Thornton and Guza* [1983, Figure 11]. Duck94 data provided by T. Lippmann for 11–12 October.

[17] Tidal variation in water level affects the percent breaking for a given bar location over a tidal cycle, for example allowing some breaking at low tide even if no breaking would be predicted at mean tide. Since the subsequent analysis is based on daily or semidaily estimates of wave forcing, these variations must be parameterized. Equation (6) was adjusted for tidal effect by replacing Γ with Γ_t:

$$\Gamma_t = \Gamma\left[1 + \gamma_b \frac{\delta_{tide}}{h_{x_c}}\right]. \tag{7}$$

The adjusted equation was based on a best fit to tidally integrated estimates of total wave breaking fraction using equation (6) for a suite of water depths, wave heights and tidal ranges (δ_{tide}).

2.2. Linking Parametric and Continuous Models of Sediment Transport

[18] Parametric models provide a simplified representation of nearshore variability and are quite useful if continuous geophysical observations can be partitioned into a few dominant modes of variability. An important part of the link was established by *Plant et al.* [2001], who analyzed 16 years of monthly beach profile data from Duck, North Carolina, to examine the relationship between changes in depth, h, and their resulting sediment transport patterns, Q_x, that caused that change using the conservation of mass equation

$$\frac{\partial h}{\partial t} = \frac{1}{\mu}\frac{\partial Q_x}{\partial x}, \tag{8}$$

where μ is the sediment packing factor of settled sediment grains. They showed that the bulk of temporal changes of the profile between consecutive surveys were due to migration of bars of nearly constant shape. *Bagnold* [1941] had shown previously the general result that for a bed form of arbitrary but unchanging shape to undergo strict migration, the associated sediment transport pattern must have the same shape as the bed form. Therefore, if we choose $Q_{x_{xc}}$ and Δ_{x_c} to be the cross-shore transport and sandbar height measured at the bar crest, x_c, then Q_x can be represented as

$$Q_x = \frac{Q_{x_{x_c}}}{\Delta_{x_c}} h. \tag{9}$$

Substituting equation (9) into equation (8), we have

$$\frac{\partial h}{\partial t} = \frac{Q_{x_{x_c}}}{\mu \Delta_{x_c}}\frac{\partial h}{\partial x}, \tag{10}$$

which is just the equation for a moving bar form where the migration rate, $\dot{x}_c$, is given by

$$\dot{x}_c = \frac{1}{\mu}\frac{Q_{x_{xc}}}{\Delta_{x_c}}. \tag{11}$$

This provides a convenient relationship between the bar migration rate, a parametric representation, and the sediment transport at the bar crest, a geophysical variable, provided the sandbar migrates without change of shape.

[19] While the *Plant et al.* [2001] result of unchanging bar shape was valid for consecutive pairs of beach surveys, when the full range of sandbar positions across the surf zone are considered, both bar height and length are expected to vary with depth [*Ruessink et al.*, 2003]. The constant form transport equation (11) can be adapted by a simple change of variables to include a cross-shore dependency without altering the underlying assumption of constant form migration:

$$\dot{x}_c = \frac{1}{\mu\Delta_o}\left(\frac{Q_{x_{xc}}}{f_{\Delta_{x_c}} f_{L_{x_c}}}\right), \tag{12}$$

where $f_{\Delta_{x_c}}$ and $f_{L_{x_c}}$ represent the cross-shore dependency of bar crest height and length scale, respectively, and Δ_o is a reference value of bar height measured at some reference location, x_o. We will assume bar height varies linearly with the surf zone width:

$$f_{\Delta_{x_c}} = \frac{x_c}{x_o}, \tag{13}$$

and cross-shore bar length varies as

$$f_{L_{x_c}} = e^{m\beta x_c}, \tag{14}$$

where $m = 0.27$ [*Ruessink et al.*, 2003].

2.3. Sediment Transport Formulation

2.3.1. The 1DH Formulation

[20] We parameterize cross-shore sediment transport rates at the bar crest, $Q_{x_{xc}}$, using the formulation similar to BBB. Based on the observations of *Gallagher et al.* [1998], we neglect the contributions due to bed load since its contribution is small in the active surf zone and due to gravity ($\tan\beta$), since $\tan\beta$ is zero at the sandbar crest. This reduces the equation to

$$Q_{x_{xc}} = \frac{K_s}{gW}\left[\left\langle |u|^3 U\right\rangle + \left\langle |u|^3 u_w\right\rangle\right], \tag{15}$$

where angle brackets and verticals signify the time average and absolute value of a quantity; u, U, and u_w are the total (i.e., cross-shore and alongshore) near-bottom velocity, depth-averaged cross-shore current, and wave orbital velocity, respectively; g is the acceleration due to gravity; W is the sediment fall velocity; and K_s is the dimensionless suspended load transport coefficient

$$K_s = \frac{\rho_w}{(\rho_s - \rho_w)} C_d \epsilon_s, \tag{16}$$

where ρ_w and ρ_s are the density of water and sediment, respectively, C_d is the drag coefficient, and ϵ_s is the suspended load efficiency factor. Following *Gallagher et al.* [1998], we set $\epsilon_s = 0.015$ and $C_d = 0.003$. W is set to 0.04 m s^{-1}.

[21] In the 1DH case, all the wave-driven shoreward fluid mass transport must be returned by the undertow, U. This fluid mass transport is composed of two contributions: the return flow due to Stokes drift, U_s, and due to the wave roller, U_r [*Svendsen*, 1984]:

$$U = U_s + U_r = \left(U_s + bc\frac{\bar{e}}{h}\right)\cos\theta, \tag{17}$$

where $\bar{e} = 0.9\ H^2/L$ is the roller thickness, H is the local RMS wave height, L is the local wavelength, c is the wave celerity, and θ is the wave angle with respect to shore normal. When only a fraction of the waves are breaking, we have modeled the contribution of the roller as being proportional to that fraction of breaking, b (section 2.1). We will assume that at the bar crest, changes in the return flow due to Stokes drift and skewness contributions stay roughly in balance leaving a residual that is related to variations in the roller term, a form similar to that proposed by *Kriebel and Dean* [1985] and *Larson and Kraus* [1989]:

$$Q_{x_{xc}} = \frac{K_s}{gW}\left[\left\langle |u|^3\left(U_{r,b} - U_{r,eq}\right)\right\rangle\right], \tag{18}$$

where $U_{r,b}$ and $U_{r,eq}$ are the roller contribution to undertow due to breaking and an equilibrium value, respectively. This simplifies to

$$Q_{x_{xc,1DH}} = \alpha_1 \hat{Q}_{x_{xc}}\left(\gamma_b - \gamma_{eq}\right), \tag{19}$$

where α_1 is a nondimensional free parameter in the model, γ_{eq} is a free parameter in the model representing the amount of relative wave breaking where onshore and offshore transport are in equilibrium and

$$\hat{Q}_{x_{xc}} = \frac{3}{5\pi} K_s b \gamma_{x_c}^3 \Omega h_{x_c}\sqrt{g h_{x_c}}\cos\theta_{x_c}. \tag{20}$$

$\Omega = H_b/TW$ is the dimensionless fall velocity term and θ_{x_c} is the wave angle with respect to the shore normal measured at the bar crest. Assuming $u_w \gg U$, the total velocity at the bar crest has been replaced by its phase-averaged shallow water form ($\langle |u|^3\rangle = (2/3\pi)\gamma_{x_c}{}^3 g h_{x_c}\sqrt{g h_{x_c}}$) [*Bowen*, 1980]. $\gamma_{x_c} = H_{x_c}/h_{x_c}$ is the relative wave height at the bar crest.

[22] During storms, wave breaking is saturated over the bar and much of the surf zone. To balance the saturated roller transport, the undertow is large and predominantly 1DH and net transport is in the offshore direction (positive values). Under calm conditions, no waves break over the bar and other processes such as skewness-based transport, boundary layer effects or bed load may dominate, but are assumed negligible compared to breaker-driven processes and the inclusion of the fraction of breaking in our formulation will result in negligible transport. Under intermediate wave conditions, partial breaking over the bar can drive sediment transport in either the onshore or offshore direction depending on the relative wave height and antecedent morphology.

2.3.2. The 2DH Formulation

[23] When morphology becomes alongshore variable, the requirement to balance wave mass transport through undertow at each cross-shore transect is removed. Instead, horizontal circulation may occur when waves approach near normal to the shore and result in onshore-directed flow over the typically broad shoals and offshore-directed flows concentrated in narrow rip channels [e.g., *Haller et al.*, 2002; *Garnier et al.*, 2008]. While fluid mass flux is still required to balance in the alongshore average, there is no such requirement for integrated sediment flux. Sediment transport is a nonlinear function of flow and the active volume of moving sediment lies close to the bed such that broad but weaker onshore flows could contribute more to transport than concentrated but deep return rip flows. Therefore, it is quite plausible that sand brought into suspension by breaking processes can be carried onshore by both the waves and onshore currents and explain the decreased skill in 1DH models in the presence of 2DH morphology [*Plant et al.*, 1999; *Ruessink et al.*, 2007].

[24] We hypothesize that the presence of 2DH morphology has two consequences on the alongshore-averaged sediment transport. First, under near-normal waves, the presence of horizontal circulation facilitates gross sediment transport (i.e., $\hat{Q}_{x_o,2DH} = f(a)\hat{Q}_{x_{x_c}}$). Second, since fluid mass transport does not need to be balanced at each cross-shore transect for an alongshore-variable system, the presence of 2DH morphology will drive alongshore variable circulation [e.g., *Feddersen and Guza*, 2003; *Reniers et al.*, 2004]. As a result, net onshore transport may continue in the presence of larger waves over 2DH sandbar morphology than over an alongshore-uniform equivalent system, shifting the equilibrium balance (i.e., $\gamma_{eq,2DH} = f(a)\gamma_{eq}$). These functionalities are implemented into equation (19) for 2DH conditions:

$$Q_{x_{x_c,2DH}} = \alpha_1 \kappa_a \hat{Q}_{x_{x_c}} \left(\gamma_b - \kappa_a \gamma_{eq}\right), \tag{21}$$

where κ_a represents the influence of 2DH processes on the alongshore-averaged cross-shore bar migration:

$$\kappa_a = 1 + \alpha_2 \frac{a}{x_c(\beta - \Delta_o/x_o)} b\zeta \frac{H_{x_c}}{H_b}, \tag{22}$$

where α_2 is a nondimensional free parameter in the model. The main objective is to capture the relative influences of existing morphology versus the incident fluid forcing and subsequent 2DH circulation. First, the presence of breaking, b, is assumed to be required to drive circulation and the effect of 2DH morphology is assumed to scale with surf zone width, a/x_c. The term $(\beta - \Delta_o/x_o)$ represents the rate at which the depth over the bar varies with cross-shore distance. Second, the size and location of breaking waves with respect to the sandbar position affect the influence of morphology on the resulting 2DH circulation. We model this by the ratio of the depth-limited wave height at the bar versus the breaking wave height, H_{x_c}/H_b, such that when waves are breaking offshore of the bar or bar crest wave heights are very small ($H_{x_c}/H_b \ll 1$), 2DH processes are reduced, while if waves are just breaking at the bar ($H_{x_c}/H_b \sim 1$) we expect the largest potential for 2DH conditions with respect to wave height. Finally, it has been commonly observed that the effect of alongshore-variable forcing or morphology becomes muted under strong alongshore currents [e.g., *Yu and Slinn*, 2003; *Wilson*, 2009], and we model this dependency using the formulation of *Wilson* [2009] (see Appendix A):

$$\zeta = \frac{1}{\sqrt{1 + Re_s^2}}, \tag{23}$$

which only depends on the "shallow water Reynolds number" [*Allen et al.*, 1996] that can be simplified to

$$Re_s = \frac{2.7}{c_f} k_y h_{x_c} \sin\theta_{x_c} \cos\theta_{x_c}, \tag{24}$$

where c_f is the wave friction factor and k_y is the alongshore wave number of alongshore variability. *Wilson* [2009] showed that as the offshore wave angle increased, the effect of alongshore bathymetric variability was damped out, reducing the alongshore variability of alongshore and, by continuity, cross-shore currents.

[25] Combining equations (21) and (12), the final equation for sandbar migration is

$$\dot{x}_c = \alpha_1 \kappa_a M \left(\gamma_b - \kappa_a \gamma_{eq}\right), \tag{25}$$

where

$$M = \frac{1}{\mu \Delta_o} \left(\frac{\hat{Q}_{x_{x_c}}}{f_{\Delta_{x_c}} f_{L_{x_c}}} \right). \tag{26}$$

2.4. Temporal Changes of 2DH Surf Zone Variability

[26] Using equations (25) and (26), forward prediction of bar position, given $a(t)$ and forcing can be obtained. We can examine the influence of 2DH processes on sandbar dynamics, but in order to study the dynamic relationship between alongshore-averaged bar position and 2DH variability of the bar, equations describing the changes in $a(t)$ are also required. Although many mechanisms have been postulated as to why sandbars develop 2DH variability [see *Coco and Murray*, 2007, and references therein], equations detailing the time evolution of variability, $\dot{a}(t)$, are not generally available. We will assume that 2DH morphology is due to self-organization processes associated with 2DH currents [e.g., *Reniers et al.*, 2004; *Drønen and Deigaard*, 2007; *Garnier et al.*, 2008] and can be modeled as an instability:

$$\dot{a} = \alpha_3 \frac{a}{a_o} MG, \tag{27}$$

where a_o is included for dimensional consistency (set to the mean value) and G parameterizes the various physical processes that potentially influence the growth and decay rate of 2DH processes:

$$G = \frac{T}{T_o} \left(1 - \frac{3a}{x_c}\right) - \alpha_4 \frac{\Omega \gamma_b}{\zeta}. \tag{28}$$

A reference value of T_o (the mean wave period) is included such that the free parameters, α_3 and α_4, are nondimensional. The timescales of growth are influenced by wave

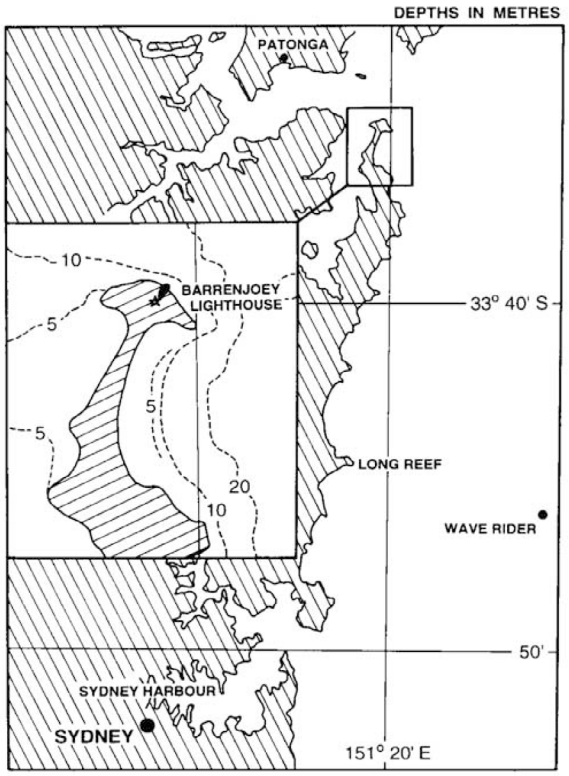

Figure 2. Map of Palm Beach, Australia.

period, T [*van Enckevort et al.*, 2004; *Calvete et al.*, 2005]. The term (1–3 a/x_c) limits growth as the landward portions of the variable bar become limited by the shoreline. Large wave angles (small ζ), as well as large waves (large Ω) breaking seaward of the bar (large γ_b) drive more 1DH hydrodynamics and return the bar back to a 1DH configuration [*Calvete et al.*, 2005; *Garnier et al.*, 2008]. We acknowledge there are many unknowns in the formulation of G and other forms may also be possible. Tidal range, δ_{tide}, has also been shown to influence the growth of 2DH morphology [*Wright et al.*, 1987] and is included in equation (27) through the tidally integrated breaking term (b) used to estimate M.

3. Data

3.1. Field Site Description

[27] Palm Beach, a 2 km long, east facing, open ocean embayment, located approximately 30 km north of Sydney, Australia (Figure 2) was chosen for the study site due to its dynamic nature, predominance of 2DH morphology and readily available images from the Argus camera network [*Holman et al.*, 2003]. The beach morphology at Palm Beach ranges from dissipative, with an alongshore uniform sandbar during major storms, through all four intermediate beach states described by *Wright and Short* [1984] during milder wave conditions. The most observed state is the transverse bar rip (55%) [*Ranasinghe et al.*, 2004]. State changes occur quite rapidly, with rhythmic sandbars and rip channels developing usually within a week of a major storm. Although no preferential rip locations were found in a study by *Holman et al.* [2006], *Alexander and Holman* [2004]

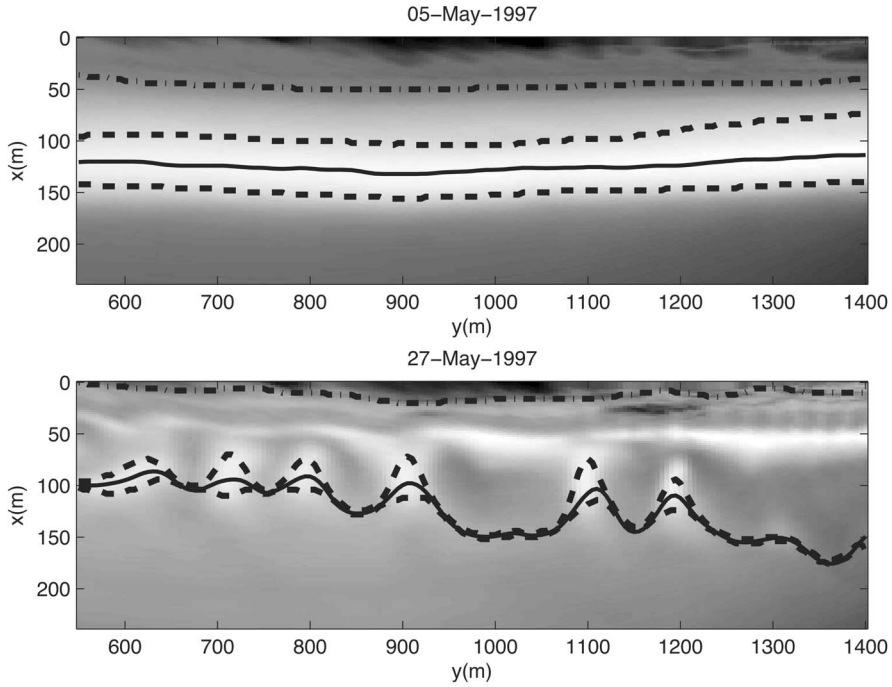

Figure 3. Example of image ranking system results. (top) Daytimex image for 5 May 1997, with sandbar position (solid), bounds of breaking (dashed), and shoreline (dash-dotted). Image was given a ranking of 9, indicating good matches for all terms. (bottom) Daytimex image for 27 May 1997. Image was given a ranking of 2, indicating features were either missed (due to lack of breaking) or falsely identified.

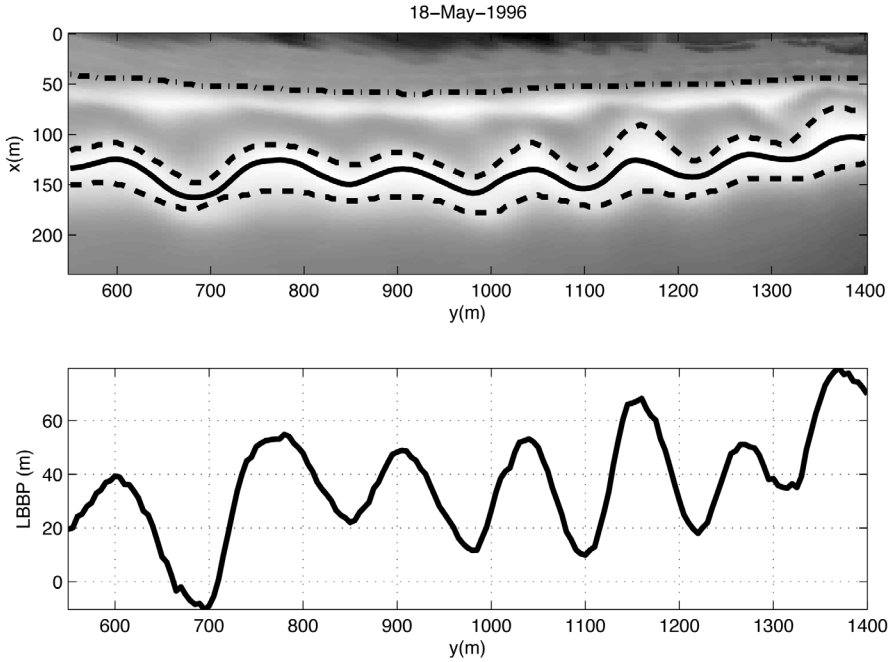

Figure 4. Example of isolating bar position and active breaking. (top) Daytimex image for 18 May 1996, with bar (solid) and breaking bounds (dashed) and shoreline (dash-dotted). (bottom) Longshore sandbar breaking profile (LBBP).

found a significant correlation between offshore significant wave height and inverse rip spacing at short lags (about a day) indicating that morphology responds very rapidly to changing wave conditions.

[28] The embayment is defined by the Barrenjoey headland to the north and the Little Head headland to the south. The nearshore beach slope, β, is 0.029 [*Wright et al.*, 1980] and the median grain size, d_{50}, is 0.30 mm [*Wright et al.*, 1980]. Based on a linear best fit to an October 1999 survey of Palm Beach, $\Delta_o/x_o = 0.0076$. The location is microtidal ($\delta_{tide} = 1$ m) and swell-dominated, with no significant seasonal variability in the wave conditions [*Short and Trenaman*, 1992]. The dominant wave direction is from the SSE with the occasional E and NE swell and wave heights averaging 1.5 m, but reaching 3–6 m during storm conditions [*Short and Trenaman*, 1992].

3.2. Wave Characterization

[29] The offshore wave characteristics (significant wave height, wave angle, and wave period) obtained from a directional wave rider buoy located at Long Reef, 20 km south of Palm Beach, in a depth of 80 m (Figure 2) were input into the 2-D Hindcasting Shallow Water Waves (HISWA) wave refraction model [*Holthuijsen et al.*, 1989] and propagated to the 10 m contour. Output was in the form of daily RMS wave heights, $H_{\mathrm{RMS},10}$, wave angle, θ_{10}, and period, T. Breaking wave heights, H_b, were calculated from *Komar* [1974] using conservation of energy flux up to a depth-limited breakpoint ($H_b/h = 0.42$) and taking into account refraction assuming Snell's law:

$$H_b = \left(\frac{0.42}{g}\right)^{1/5} \left(H_{\mathrm{RMS},10}^2 C_{g,10} \frac{\cos\theta_{10}}{\cos\theta_b}\right)^{2/5}, \qquad (29)$$

where $C_{g,10}$ is the group velocity measured at 10 m and θ_b is the breaking wave angle with respect to the shoreline. Similarly, the equivalent unbroken wave heights at the bar location were calculated using linear wave theory, Snell's law, and conservation of energy flux [e.g., *Dean and Dalrymple*, 1991]. Wave heights defined at the bar crest, H_{x_c}, were set to the minimum of the unbroken wave height at the bar (representing a shoaling wave), the breaking wave height (a wave just breaking at the bar) or 0.6 h (a fully breaking wave); 0.6 h was chosen as the maximum stable RMS wave height allowed for a broken wave propagating into shore.

3.3. Beach Characterization

3.3.1. Video Data

[30] A two-camera Argus video-imaging station [*Holman et al.*, 2003] was installed in the Barrenjoey lighthouse in January 1996 (Figure 2). The cameras are located 115 m above mean sea level and face south toward Palm Beach. Only the wide-angle lens camera, C1, is used in this study as it provides a view of 90% of the study area. Daytimex images (images showing the average of all 10 min time exposure images from any particular day) were rectified to an overhead (plan) view using standard photogrammetric

Table 1. Definition of the Traditional 1DH Model and the 2DH Model Setups Used

Mode	Model Setup
1DH	$\dot{x}_c = f(H_{\mathrm{RMS},10},T,\theta_{10})$
2DH uncoupled	$\dot{x}_c = f(\hat{x},a,H_{\mathrm{RMS},10},T,\theta_{10})$
2DH dynamically coupled	$\dot{x}_c = f(\hat{x},\ \hat{a},\ H_{\mathrm{RMS},10},T,\theta_{10})$
2DH dynamically coupled	$\dot{a} = f(\hat{x},\ \hat{a},H_{\mathrm{RMS},10},T,\theta_{10})$

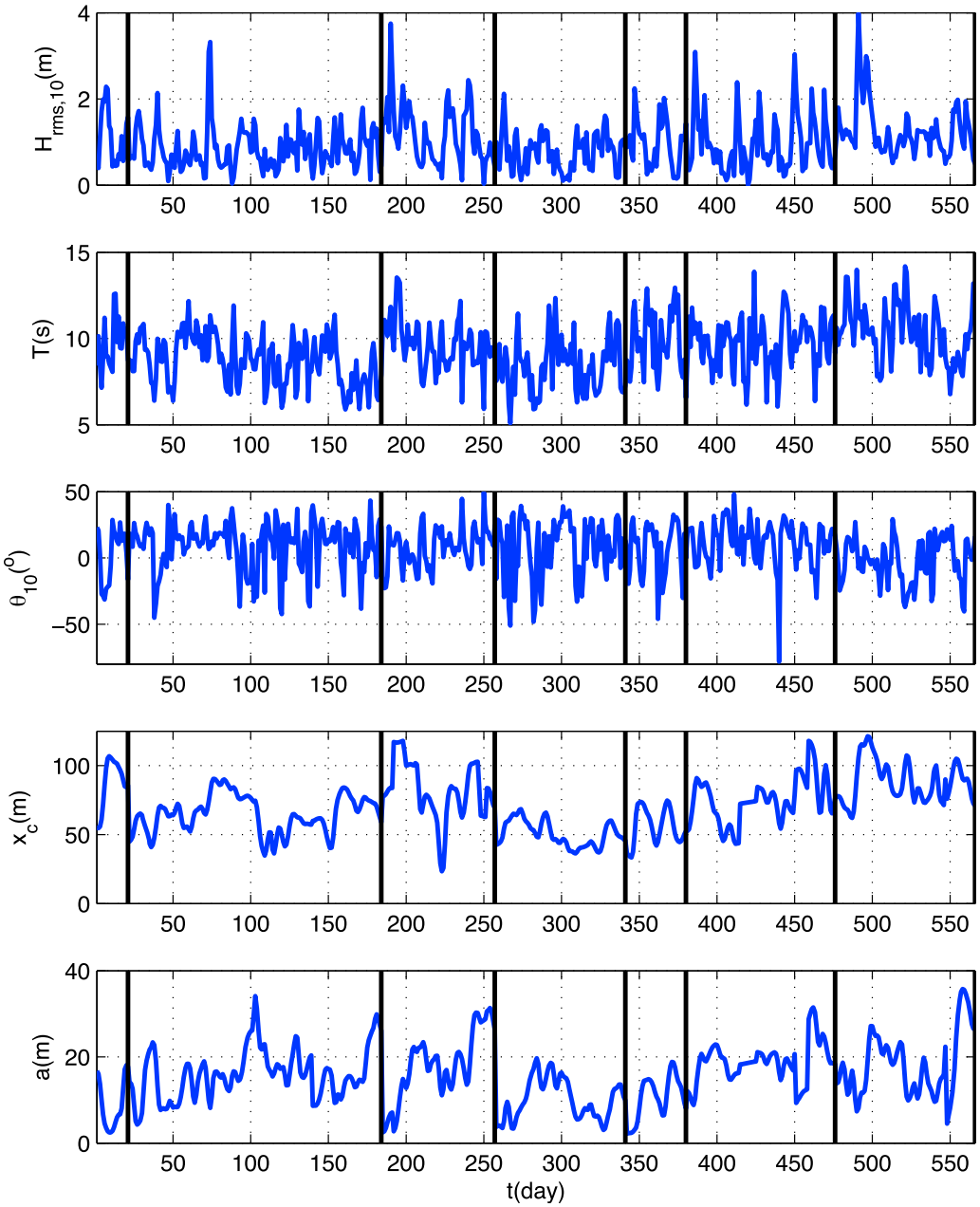

Figure 5. Summary of data collected over 4 years at Palm Beach, Australia. Data have been concatenated, and vertical lines represent breaks between data sets.

transformations [*Holland et al.*, 1997]. The curved shoreline at Palm Beach was transformed to a straightened coordinate system following the method and values of *Alexander and Holman* [2004]. To account for lighting artifacts in the image due to grazing angle and to enhance the contrast between breaking and nonbreaking, each daytimex image was adjusted based on the methods of *Splinter* [2009].

[31] Each image was subjectively ranked from 0 to 9 and then given a normalized weighting, w, indicating the quality of the algorithms at capturing the bar position, shoreline, and breaking patterns. K. Splinter and R. Holman independently ranked the images a total of 4 times, with comparable results (mean R^2 = 0.81). An example is shown in Figure 3.

3.3.2. Alongshore-Averaged Sandbar Position

[32] Daily sandbar positions, $x_{bar}(y,t)$, were obtained from images by exploiting preferred wave breaking patterns that correspond to topographical highs, such as sandbars [e.g., *Lippmann and Holman*, 1989]. Bar positions were estimated at 5 m intervals in the alongshore direction using a bar line intensity maximum (BLIM) tool that searches for the local intensity maximum in a cross-shore intensity profile within a user defined region of interest (Figure 3). Shoreline positions, $x_s(y,t)$, were determined based on the method of *Alexander and Holman* [2004]. Mean sandbar position, x_c,

Table 2. Data Set Statistics Used in Analysis, Including Major Storm Resets as Defined by *Holman et al.* [2006]

	Number of Days	Number of Resets	$\overline{H}_{\mathrm{RMS},10}$ ($\sigma_{H\mathrm{RMS},10}$) (m)	$\overline{T}$ (σ_T) (s)	$\overline{\cos\theta_{10}}(\sigma_{\cos\theta_{10}})$
April 1996	21	1	1.13 (0.61)	9.67 (1.31)	0.94 (0.04)
July 1996	163	4	0.84 (0.49)	8.72 (1.44)	0.94 (0.06)
May 1997	73	1	1.18 (0.68)	9.66 (1.43)	0.96 (0.06)
October 1997	84	1	0.77 (0.42)	8.39 (1.54)	0.92 (0.08)
March 1998	39	1	0.97 (0.53)	9.85 (1.78)	0.94 (0.06)
May 1998	96	2	0.96 (0.65)	9.73 (1.48)	0.94 (0.10)
April 1999	90	1	1.27 (0.61)	10.35 (1.68)	0.96 (0.05)

was defined as the alongshore-averaged cross-shore distance between x_{bar} and x_s.

3.3.3. Surf Zone Variability

[33] Surf zone variability, $a(t)$, is a proxy for 2DH currents that are a function of the bathymetry and the incident wavefield. *Plant et al.* [2006] proposed a method to estimate $a(t)$ based on the band-passed root mean variance of the alongshore bar position that works well when sandbars are offshore and breaking over the bar is relatively alongshore uniform. As the morphology becomes more 2DH (developing shoals and rips, i.e., Figure 4), the alongshore variability of breaking should also influence the expected 2DH circulation and needs to be accounted for. Landward and seaward limits to the region of active breaking were defined by first exceedances of intensity above a threshold of 0.8 times the maximum intensity at x_{bar}, and subsequently smoothed with a 50 m Hanning filter to remove small-scale variations (Figure 4). Similar to *Ranasinghe et al.* [2004], the longshore intensity profile, LIP(y,t), was found by cross-shore integration of intensities between these limits. Finally, a composite longshore bar breaking profile, LBBP, combining bar crest position and breaking intensity information was defined as

$$\mathrm{LBBP} = x_c - x_{bar} + \mathrm{LIP}. \tag{30}$$

[34] Surf zone variability was calculated using daily estimates of LBBP (Figure 4) based on the spectral method described by *Plant et al.* [2006] with a bandpass between 30 and 400 m based on the length scales over which we assume 2DH processes to be important at Palm Beach.

3.4. Model Evaluation

[35] Seven data sets representing a subset of the 4 years of data presented by *Alexander and Holman* [2004] and *Holman et al.* [2006] were used to test model equations (25) and (27). The model was initially started from known x_c and $a(t)$ for each data set and forward predictions in time (dt = 1 day) were based on a fourth-order Runge-Kutta scheme [*Durran*, 1999]. Modeled sandbar position, $\hat{x}(t)$, and 2DH variability, $\hat{a}(t)$, were compared against measured values. The 2DH model was run in two different modes (Table 1) to test the effect of various levels of coupling and feedbacks. Although both 2DH models involve some level of coupling between x_c and a, we have defined the uncoupled model to mean the derivative equations are not dynamically linked to each other. Data sets varied in length from 1 to 6 months, totaling 566 days and covered a full range of conditions. All data sets included at least one major storm and in most cases also contained several minor storms where full resets did not occur. Data are plotted in Figure 5, and general statistics are summarized in Table 2.

[36] Four different measurements were computed to evaluate the model skill: the squared correlation coefficient, R^2, the root mean square error, RMSE, the Brier skill score, BSS, and the relative bias, B. Data with a weighting, w, greater than or equal to 7 (of 9) were used to calculate model-data comparison statistics. The Brier skill score is calculated as

$$\mathrm{BSS} = 1 - \frac{\mathrm{var}(\mathrm{model} - \mathrm{data})}{\mathrm{var}(\mathrm{data})}, \tag{31}$$

where a BSS = 1 is a perfect skill and a BSS = 0 means the model has no skill. A value less than zero indicates the model is worse than predicting no change at all. The relative bias is calculated as

$$B = \frac{\langle \mathrm{model} - \mathrm{data} \rangle}{\max(\mathrm{RMS}_m, |\langle \mathrm{data} \rangle|)}, \tag{32}$$

where angle brackets indicate an average and RMS_m is the root-mean-square of the model result.

4. Results

4.1. Model Calibration

[37] There are five free parameters (α_1–α_4 and γ_{eq}) for which appropriate values must be chosen. Based on the fact

Table 3. Global Best Fit Calibration Coefficients ±95% Confidence Intervals and Statistics for 2DH Models

	Uncoupled	Dynamically Coupled
α_1	1.25 ± 0.13	1.66 ± 0.13
α_2	0.08 ± 0.005	0.08 ± 0.003
α_3	-	3.18 ± 0.96
α_4	-	0.04 ± 0.004
$R_{x\hat{x}}{}^2$	0.46	0.49
RMSE_x (m)	12.53	11.77
BSS_x	0.40	0.42
B_x	0.00	0.00
$R_{a\hat{a}}{}^2$	-	0.41
RMSE_a (m)	-	5.06
BSS_a	-	0.40
B_a	-	0.02

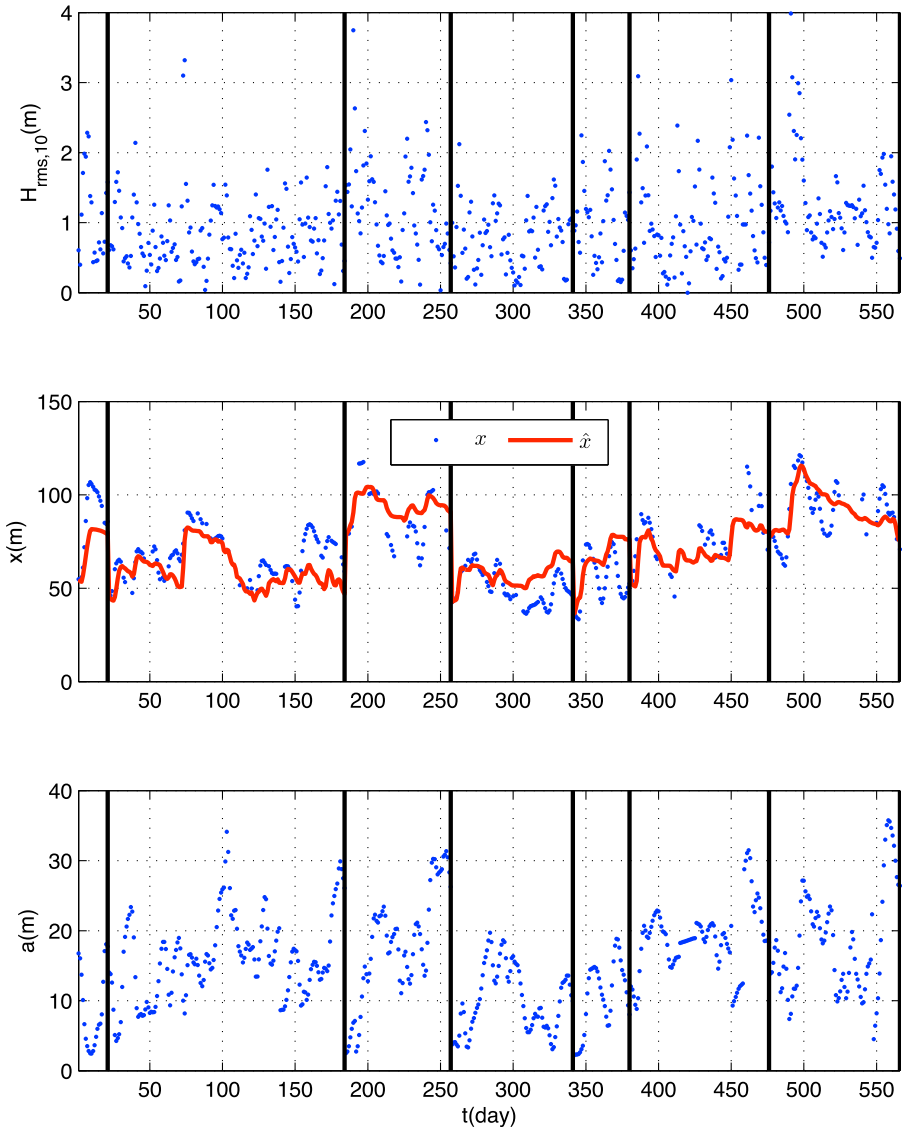

Figure 6. Results for uncoupled model. All data have been concatenated, and vertical thick black lines indicate the start of a new data set and a reset of x_c (Table 2). Model skill was $R_{\dot{x}\dot{x}}^2 = 0.46$. (top) RMS wave height measured at 10 m depth, $H_{\mathrm{RMS},10}$, (middle) bar position, x_c (m), and (bottom) 2DH bar variability, $a(t)$ (m). Raw data (circle) and model predictions (line) are shown.

that $\gamma_{eq} = H_b/h_{x_c}$ represents the equilibrium amount of wave breaking, a value of 0.65 was chosen based on a sensible range of expected values and matching overall rates and magnitudes of offshore migration when $\kappa_a \approx 1$ and only 1DH processes were considered. Testing values $0.45 < \gamma_{eq} < 0.9$ showed minimal increase in model skill for increasing values of γ_{eq} due to the nonlinear form of the model where variations in γ_{eq} are compensated by α_2 in the calibration processes. α_1 and α_3 represent overall magnitude terms, while α_2 indicates the influence of $a(t)$ on $\dot{x}_c$, and α_4 balances relative growth and decay of $a(t)$. α coefficients for both the uncoupled and dynamically coupled model were calculated based on a weighted nonlinear least squares solution for the entire data set (Table 3). The weighting scheme was based on image quality as described in section 3.3.1.

4.2. Uncoupled Model

[38] Model-data comparisons for equation (25) are presented in Figure 6, and performance statistics for the entire data set are given in Table 3. The uncoupled model had an overall Brier skill score of 0.40 and a relative bias of 0.003, indicating model error variance was small compared to measured variance. Comparison of model-data cross spectra (not shown) indicated sandbar position was well modeled (significantly coherent) for time periods longer than 9 days. Using the global model coefficients (Table 3), equation (25) had significant skill at predicting the time evolution of $\hat{x}(t)$ for all of the individual data sets (Table 4). The results from July–December 1996 are presented in Figure 7 and show good agreement between measured and modeled sandbar position. In all cases, the Brier skill score indicated the 2DH model had some level of skill and did better than predicting

Table 4. R^2, RMSE, Brier Skill Score, and Relative Bias Statistics for Uncoupled Model Using the Global Best Fit Model Coefficients[a]

Data Set	$R_{x\hat{x}}^2$	$\text{RMSE}_{x\hat{x}}$ (m)	BSS	B
April 1996	0.85	17.8	0.74	−0.16
July 1996	0.46	11.7	0.43	−0.11
May 1997	0.63	13.1	0.46	0.07
October 1997	0.21	11.5	0.16	0.15
March 1998	0.25	17.0	0.08	0.20
May 1998	0.64	11.8	0.62	−0.09
April 1999	0.50	11.1	0.50	0.02

[a]See Table 3.

no change at all. The low skill for the March 1998 data set was due to very low measured values of $a(t)$ due to the presence of terraces and as a result, very little onshore migration was predicted in the model.

4.3. Dynamically Coupled Model

[39] By coupling the equations for sandbar migration and 2DH variability we were able to examine the dynamic relationship between the two terms. Model-data comparisons for the dynamically coupled equations (25) and (27) are presented in Figure 8, and performance statistics are given in Table 3. Model skill for sandbar position was slightly higher than for the uncoupled model and comparison of model-data cross spectra was similar to the uncoupled model. 2DH variability was modeled with significant skill and was coherent for timescales longer than 9 days. Modeled offshore migrations were associated with high waves and a reduction in $a(t)$, while onshore bar migration rates were linked to increasing values of $a(t)$. The growth of $a(t)$ was limited by the surf zone width (i.e., when the ratio of $3\ a/x_c \sim 1$), realistically constraining the positive feedback between sandbar position and 2DH variability. Larger values of $a(t)$ maintained the bar system closer to shore, agreeing well with observations that highly 2DH systems do not migrate offshore due to slight increases in wave height. The dynamic model did surprisingly well on some of the more complex data sets (those spanning multiple storms), suggesting it can be used to predict nearshore bar evolution over multiple storm periods using external wave parameters. Comparing Tables 4 and 5 we find the coupled model did not consistently outperform the uncoupled model. Decreases in model skill were due to the low skill at predicting $a(t)$. The dynamic model smoothed out derivatives by limiting the influence of large changes in wave breaking on modeled $a(t)$ and in some instances, the dynamic model also limited the growth of $a(t)$ because of the surf zone width constraint in the equation. The most notable increase in skill was for days 300–345 (Figure 8), where the observations showed low-tide terraces (low values of $a(t)$) and the dynamic model predicted larger values of $a(t)$ resulting in better sandbar position agreement.

[40] Using the global model coefficients (Table 3) the model showed good skill at predicting x_c and $a(t)$ (Table 5). Figure 9 presents the results from the April–May 1996 storm event, showing excellent predictive skill at modeling the temporal variability of both sandbar position and 2DH variability. The April–July 1999 data set showed no skill at

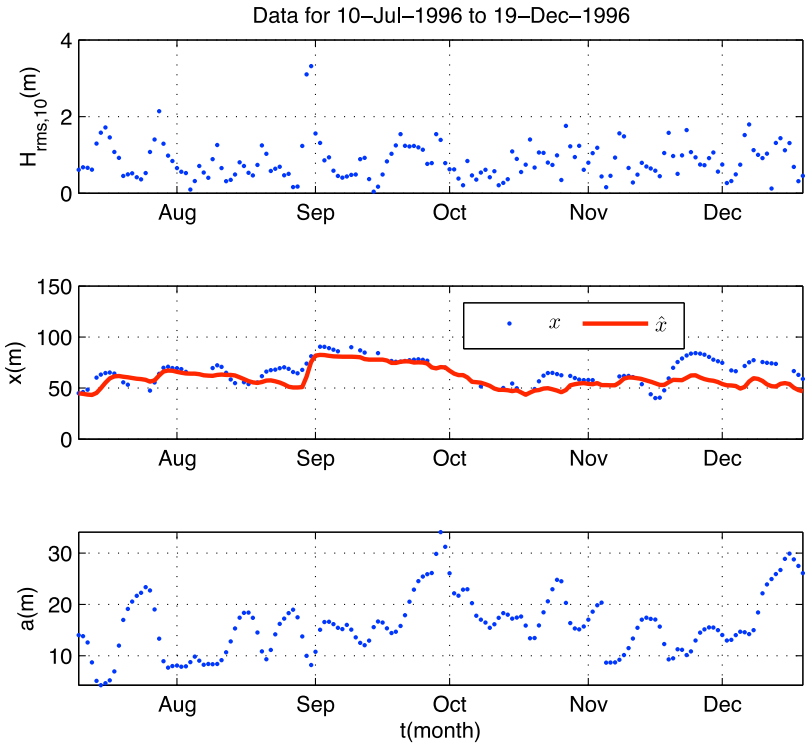

Figure 7. Results for forward testing of $\dot{x}_c$ using uncoupled model for July-December 1996. Model skill was $R_{x\hat{x}}^2 = 0.46$. (top) RMS wave height measured at 10 m depth, $H_{\text{RMS},10}$, (middle) bar position, x_c (m), and (bottom) 2DH bar variability, $a(t)$ (m). Raw data (circle) and model predictions (line) are shown.

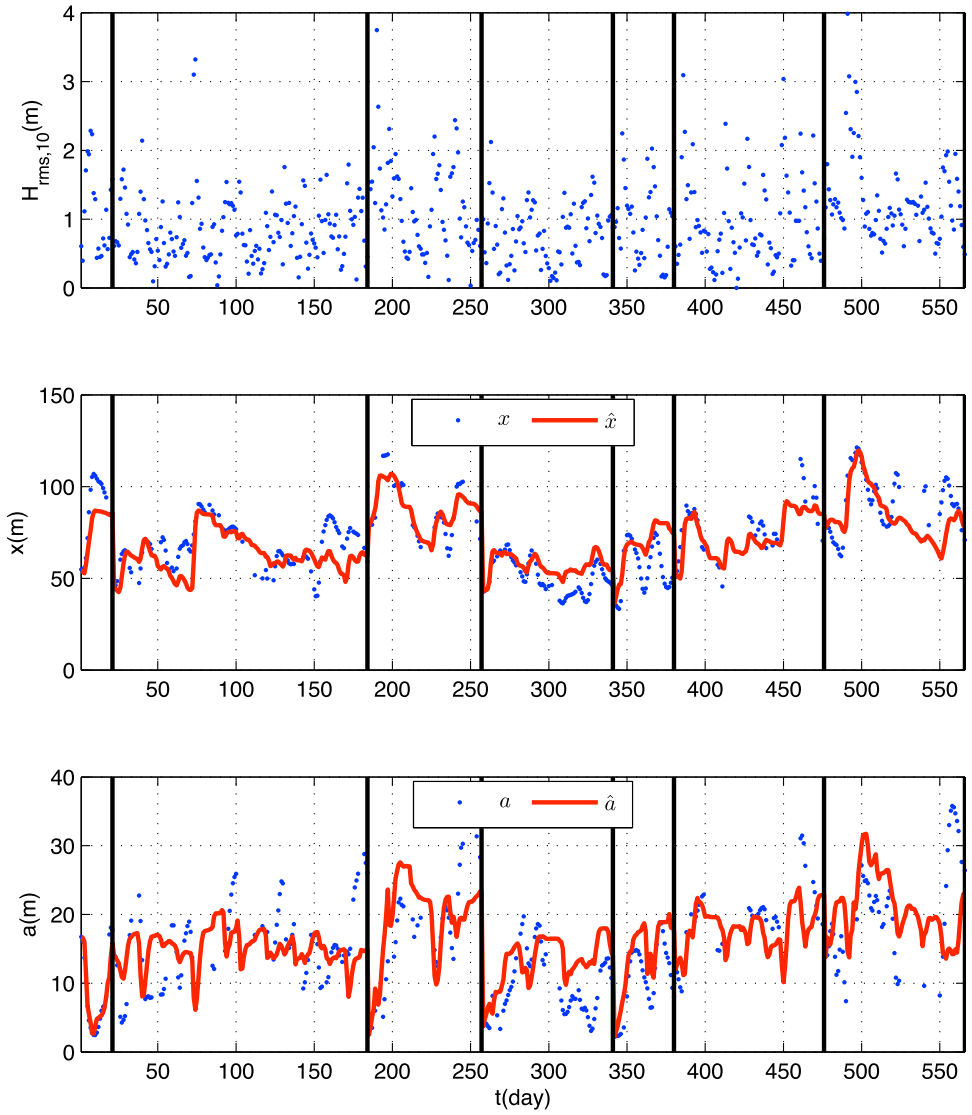

Figure 8. Model results for dynamically coupled equations. Data have been concatenated, and vertical lines represent breaks between data sets and a reset of x_c and $a(t)$. The model skill was $R_{x\hat{x}}^2 = 0.49$, $R_{a\hat{a}}^2 = 0.41$. (top) RMS wave height measured at 10 m depth, $H_{\mathrm{RMS},10}$, (middle) bar position, x_c, and (bottom) 2DH bar variability, $a(t)$. Raw data (circle) and model predictions (line) are shown.

predicting $a(t)$ and had a Brier skill score indicating it did worse than predicting no change at all. However, if we examine this closer, the first half (April–May 1999) showed good model-data agreement ($R_{x\hat{x}}^2 = 0.77$, $R_{a\hat{a}}^2 = 0.58$), but in the presence of shore-attached alongshore oblique bars the model skill decreased over the latter half of the data set.

5. Discussion

5.1. Linking Continuous and Parametric Models

[41] Parametric models offer a simplified view of the complex nearshore system and are particularly useful for understanding the relationships between forcing and sediment transport. They are simple and efficient, requiring knowledge of bulk terms rather than continuous variables and in turn reduce the sensitivity of small errors on the final result. However, their shortcoming is the potential lack of direct physical interpretation of the model drivers [*Plant et al.*, 1999, 2006; *Pape et al.*, 2010a]. Here we merge parametric and physics-based approaches. Sediment transport is modeled using energetics-based equations (BBB-type) and

Table 5. R^2, RMSE, Brier Skill Score, and Relative Bias Statistics for Dynamically Coupled Model Based on Global Best Fit Model Coefficients[a]

	x				a			
Data Set	$R_{x\hat{x}}^2$	$\mathrm{RMSE}_{x\hat{x}}$ (m)	BSS_x	B_x	$R_{a\hat{a}}^2$	$\mathrm{RMSE}_{a\hat{a}}$ (m)	BSS_a	B_a
April 1996	0.85	13.67	0.81	−0.12	0.88	2.04	0.88	−0.01
July 1996	0.33	11.66	0.23	−0.08	0.11	5.35	0.11	−0.05
May 1997	0.83	7.88	0.76	0.00	0.39	6.10	0.34	0.10
October 1997	0.58	9.06	0.56	0.13	0.27	5.38	0.22	0.33
March 1998	0.33	18.01	0.21	0.24	0.73	4.57	0.70	0.30
May 1998	0.65	10.01	0.65	−0.06	0.24	4.79	0.23	−0.08
April 1999	0.34	14.28	0.22	−0.04	0.00	9.33	−0.50	0.04

[a]See Table 3.

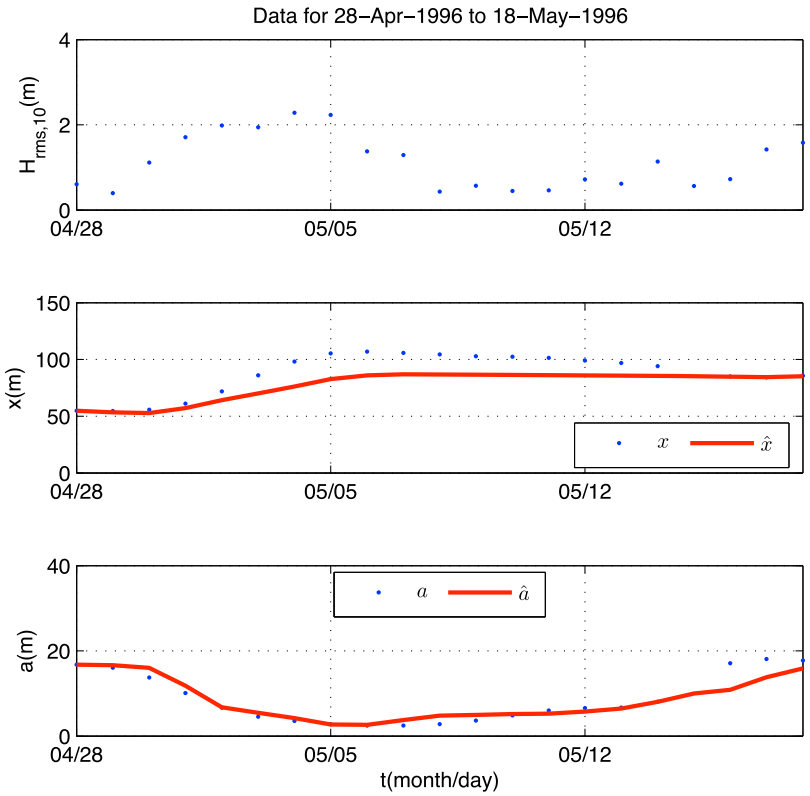

Figure 9. Results for forward testing of the dynamically coupled 2DH model for April–May 1996. Model skill was $R_{x\hat{x}}^2 = 0.85$ and $R_{a\hat{a}}^2 = 0.88$. (top) RMS wave height measured at 10 m depth, $H_{\mathrm{RMS},10}$, (middle) bar position, x_c, and (bottom) 2DH bar variability, $a(t)$.

related to a parametric form of sandbar migration based on the relationship between bar migration of a constant form and the resulting sediment transport pattern [*Bagnold*, 1941; *Plant et al.*, 2001]. Although an attempt was made to account for spatially varying sandbar volume, the main weakness of the presented formulation is estimating bar volume near the shoreline, where the morphology may no longer be classified as a distinct sandbar, but rather large shoals and incised rip channels. In an alongshore-averaged sense, the "sandbar" may not decrease in both height and length as much as our formulation would suggest. Under these circumstances, migration may be over estimated as a result of the underestimation of alongshore-averaged bar volume of the shoals.

[42] The extension of the BBB-based 1DH sediment transport equation to 2DH cannot be similarly derived from simple heuristic arguments. Instead, assumptions of the form of $a(t)$, as well as its influence on cross-shore transport processes are required. The parameterizations used in the model are extensions based on observations and previous work of onshore bar migration under 2DH morphology [*Plant et al.*, 2006] and examining the feedbacks between incident forcing and morphology [*Wilson*, 2009]. Despite these simplifications and acknowledged data and model limitations, the equations show strong skill at modeling a wide variety of conditions for extended periods of time.

5.2. Modeling Sandbar Migration

[43] An important improvement over similar previous models that use an equilibrium approach such as that of *Plant et al.* [1999, 2006] and *Pape et al.* [2010b] is the physically based dependence of transport magnitude, $\hat{Q}_{x_c}$, (and hence morphologic response) on wave breaking requiring transport to be negligible under nonbreaking conditions, even when a disequilibrium ($\gamma_b - \kappa_a\gamma_{eq}$) would otherwise drive onshore migration (i.e., Figure 10, during late May to mid-June). This agrees well with video observations when temporal gaps of breaking over the bar result in minimal bar movement.

[44] We examined the importance of including 2DH terms by selectively omitting κ_a from equation (21) in the uncoupled model. We tested the influence of the magnitude component ($\kappa_a M$), the equilibrium component ($\gamma_b - \kappa_a\gamma_{eq}$) and omitting both (i.e., a 1DH version where no influence of 2DH processes were included, Table 1). Results are summarized in Table 6. The 1DH and $\kappa_a M$ models rarely predicted onshore migration (Figure 11). For the $\kappa_a M$ model, the nonlinear best fit for the data forced $\alpha_2 = 0$ indicating the influence of 2DH processes on the magnitude component of transport was negligible. These models had a Brier skill score of −0.12, indicating they were worse than predicting no change at all. In contrast, κ_a highly influenced the equilibrium balance and captured both onshore and offshore migration events with a high degree of accuracy (Figure 11). In agreement with observations, the impact of growing 2DH morphology and roughly near-normal waves (i.e., larger values of κ_a) resulted in onshore sandbar migration under continuous breaking and self-stabilization closer to shore. The full 2DH model had the highest skill of the four models tested, allowing

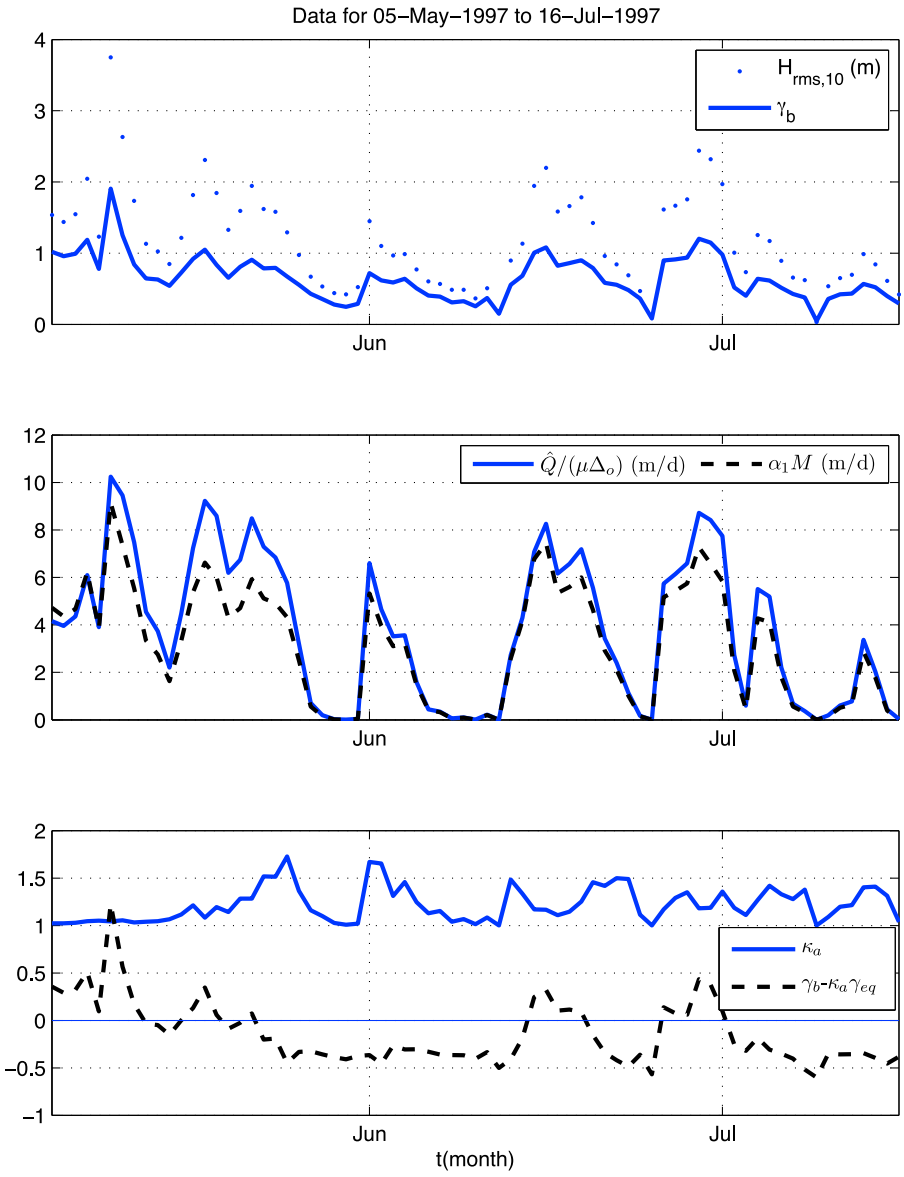

Figure 10. Comparison of wave statistics ($H_{\mathrm{RMS},10}$ and γ_b) with transport rates ($\hat{Q}$ and M) and 2DH terms (κ_a) and disequilibrium ($\gamma_b - \kappa_a\gamma_{eq}$). Vertical axes represent magnitude of modeled terms. Units are given in legend where applicable.

for both a shift in the equilibrium and an increase in the magnitude component under 2DH conditions.

[45] We found the maximum influence of κ_a to be for midrange breaking ($0.5 < \gamma_b < 1$) with negligible influence at low (<0.3) and high (>1.5) values. In the presence of 2DH morphology, predicted onshore migration rates using the 2DH model were significantly larger than those predicted using the 1DH version. Binning modeled migration rates as a function of γ_b and then plotting the median value, we determined maximum onshore migration rates for the 2DH model were on the order of 1 m d^{-1}, while the 1DH model had maximum onshore migration rates of order 0.04 m d^{-1} (Figure 12). Onshore migration was also predicted in the 2DH model for $\gamma_b < 0.9$, while the 1DH model predicted onshore migration for $\gamma_b < 0.6$. This implies 2DH processes strongly influence temporal variability of the sandbar at this site, such that when waves break over 2DH morphology and display similar breaking patterns as observed in time exposure imagery, antecedent morphology governs the system response (i.e., hysteresis). When waves become too large or too oblique (i.e., $\kappa_a \sim 1$), the effect of 2DH morphology is muted and 1DH dynamics govern the response.

5.3. Modeling 2DH Processes

[46] The proxy for 2DH processes, measured through $a(t)$, is more difficult to capture as the relationship between breaking patterns and the induced 2DH circulation is not well understood. For this reason, the parametric constraints on modeling $a(t)$ were less rigorous. For instance, terrace morphologies, often incised with rip channels, were difficult to represent through a single representation of bar sinuosity [*Plant et al.*, 2006]. Narrow channels in an otherwise alongshore-uniform system can have small values of $a(t)$, but not necessarily negligible 2DH circulation. We attempted to

Table 6. Comparison of Skill Values, RMSE, Brier Skill Score, and Relative Bias Statistics for 1DH, 2DH, and κ_a Tests[a]

	Model	α_1	α_2	$R_{x\hat{x}}^2$	$\mathrm{RMSE}_{x\hat{x}}$ (m)	BSS	B
1DH	$\dot{x}_c = \alpha_1 M(\gamma_b - \gamma_{eq})$	0.34	-	0.16	14.78	−0.12	−0.01
κ_a *Mag*	$\dot{x}_c = \alpha_1 \kappa_a M(\gamma_b - \gamma_{eq})$	0.34	0	0.16	14.78	−0.12	−0.01
κ_a *Eqm*	$\dot{x}_c = \alpha_1 M(\gamma_b - \kappa_a \gamma_{eq})$	1.36	0.09	0.38	12.47	0.37	0.01
2DH	$\dot{x}_c = \alpha_1 \kappa_a M(\gamma_b - \kappa_a \gamma_{eq})$	1.25	0.08	0.46	12.53	0.40	0.00

[a]The 2DH model was run in uncoupled mode.

capture these physics through a combined measure of 2DH bar morphology and wave breaking patterns. Due to the sensitivity of the measurement of $a(t)$ on wave conditions (namely the presence of breaking), large artificial changes in $a(t)$ could occur from day to day. As equation (27) modeled the rate of change of $a(t)$, this term was not as robust at predicting the evolution of $a(t)$ due to rapid variation in breaking and is also indicated in a drop in coherency of the model-data cross spectra for short time periods (less than 9 days). Under continuous breaking, such as is the April–May 1996 data set, the model had significant skill at predicting this term (Table 5). However, the model failed to reproduce the time variation of $a(t)$ for the April–July 1999 data set. The model was capable of reproducing $a(t)$ throughout April–May 1999 with significant skill ($R_{a\hat{a}}^2 = 0.58$) when the bar was offshore. Mild wave conditions and the growth of alongshore oblique bars throughout June and July 1999 were not accurately modeled and caused overall model skill to decrease. This is to be expected as the parameterization of equation (27) did not account for such processes and is an acknowledged limitation. Explaining the evolution of 2DH morphology has been a long-standing challenge and further work isolating the main contributors will improve this part of the model.

5.4. Dynamic Coupling

[47] The dynamically coupled 2DH model was tested under a variety of constant wave conditions ($H_{\mathrm{RMS},10}$, T, θ_{10}) starting from a number of initial states (x_c ($t = 0$) and $a(t = 0)$) to examine model sensitivity and theoretical equilibrium relationships. While the 1D model of *Pape et al.* [2010b] showed sandbars could be unstable under low wave heights,

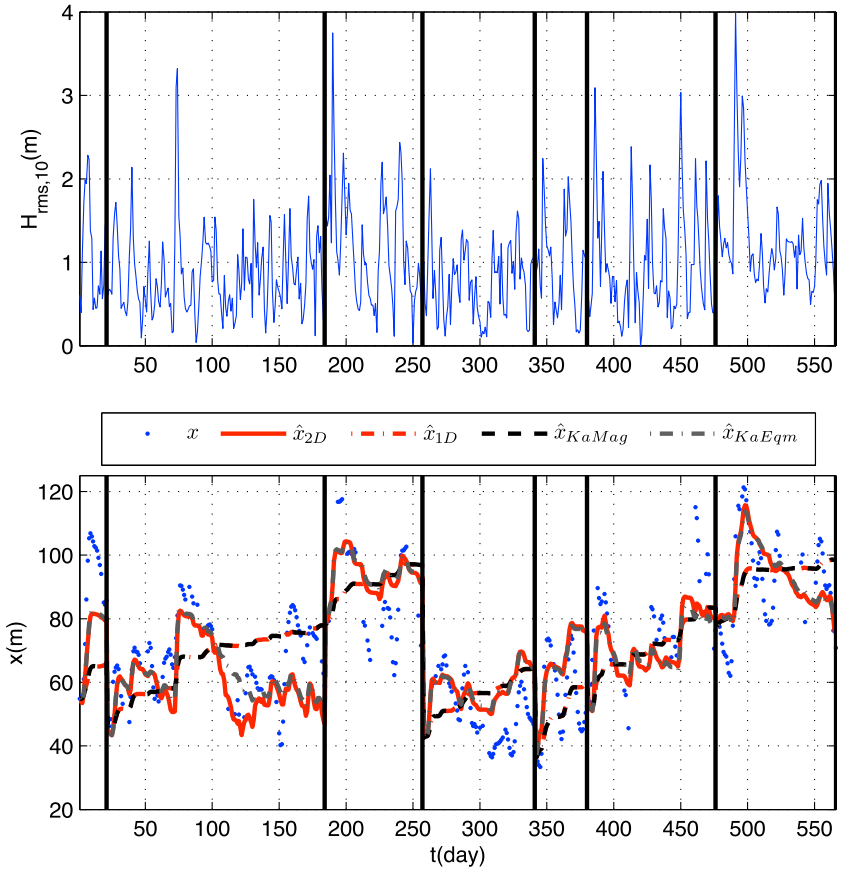

Figure 11. Comparison of κ_a influence on overall magnitude and on equilibrium balance of transport. Data have been concatenated, vertical lines represent breaks between data sets, and x_c was reset to measured value. Each model is calibrated to best fit data (Table 6).

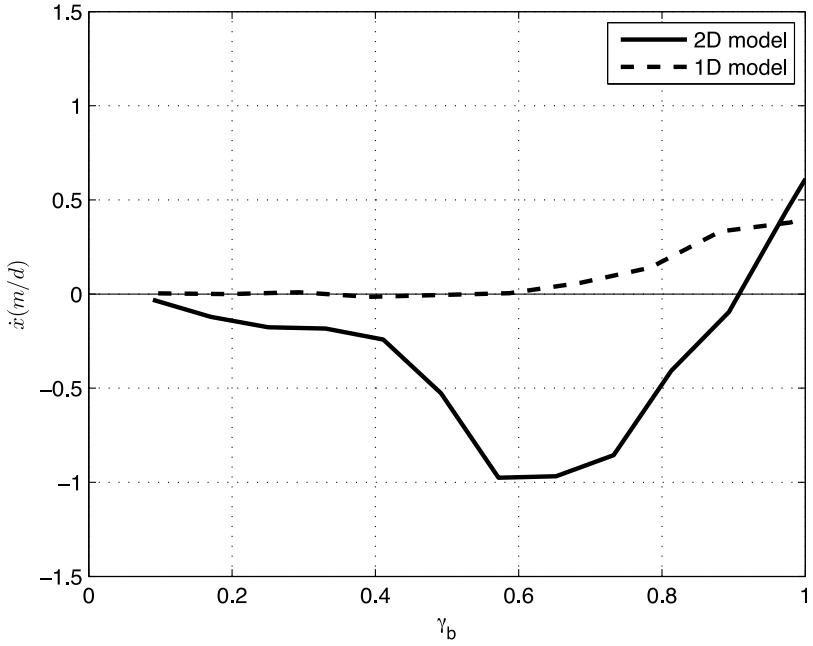

Figure 12. Comparison of median migration rates versus γ_b for the 2DH (equation (21)) and 1DH model (equation (19)). The α coefficients are best fit to each model.

the 2DH coupled model of *Plant et al.* [2006] and the results presented here show no such instability. Unlike *Pape et al.* [2010b], if initial sandbar position was way offshore of equilibrium for the given wave height [see *Pape et al.*, 2010b, Figure 3], sandbar position and 2DH variability remained constant in our model due to the requirement of some minimum value of wave breaking over the bar to drive sediment transport and 2DH circulation. Our result describes the observation of poststorm stranding of offshore sandbars. When waves were able to break over the bar and drive sediment transport, final sandbar position and 2DH variability were insensitive to initial states and equilibrium states were dictated by the input wave conditions. Comparing a range of wave heights, periods, and wave angle, we found that equilibrium sandbar position was influenced mainly by wave height, in agreement with observations and previous modeling efforts [*Plant et al.*, 1999; *Pape et al.*, 2010b], while wave period (which had not been introduced in any prior studies) had minimal effect. Shore normal waves resulted in equilibrium bar positions that were onshore of the positions for oblique waves (Figure 13a). Equilibrium 2DH variability was limited by wave period and wave angle, with shorter period and more oblique waves producing reduced 2DH variability for the same wave height (Figure 13b). This agrees with model results of *Drønen and Deigaard* [2007] and *Calvete et al.* [2005], who showed increasing alongshore length scales of 2DH morphology (i.e., a reduction in $a(t)$) under oblique waves. *Wilson* [2009] showed oblique waves significantly reduce the effect of 2DH bathymetry on the resulting hydrodynamics, and we would expect 2DH bathymetry to be reduced as a result. In qualitative agreement with *Calvete et al.* [2005] and data observations, under shore (or near)-normal waves when alongshore currents are weak, increasing wave heights resulted in the model predicting offshore bar positions and growth of 2DH morphology. For low waves, when currents are generally weak, the presence of 2DH morphology under oblique waves maintains qualitative agreement with observations [*van Enckevort et al.*, 2004].

5.5. Variability in Calibration Coefficients

[48] The model coefficients were chosen based on a weighted nonlinear least squares to the entire data set. Calibrating the model to individual data sets produced slightly improved results (Table 7). Variations in α_1 and α_3 that dictate the over rates of change were most pronounced. For example, April–May 1996, α_1 and α_3 more than doubled over the calibration coefficients from the entire data set. This was the most extreme case when a bar moved offshore and completely reset and slowly moved onshore and developed 2DH features over a period of weeks. Variations in α_2, the term describing the influence of $a(t)$ on $\dot{x}_c$ also had significant variability, with a maximum of $\alpha_2 = 0.21$ for the March 1998 data set that resulted in a significant increase in model skill for x_c (comparing Tables 4, 5, and 7). This was the case where a highly terraced system (low $a(t)$) reset under a storm but was almost instantaneously highly terraced again and quickly moved back onshore. The higher value of α_2 may indicate we did not accurately capture the 2DH processes in our estimation of $a(t)$. Despite these variations in α values, model-data correlations were similar for most of the data sets. Thus, while our derivation attempted to resolve more processes than had been done in earlier attempts, the required parameter variability implies that additional processes must be resolved in order to capture a unified model of sandbar morphodynamics.

6. Conclusions

[49] A new nonlinear model has been developed to study sandbar response to changing wave forcing. Starting with a well-known sediment transport equation that is continuous in space, a parametric form has been derived under the

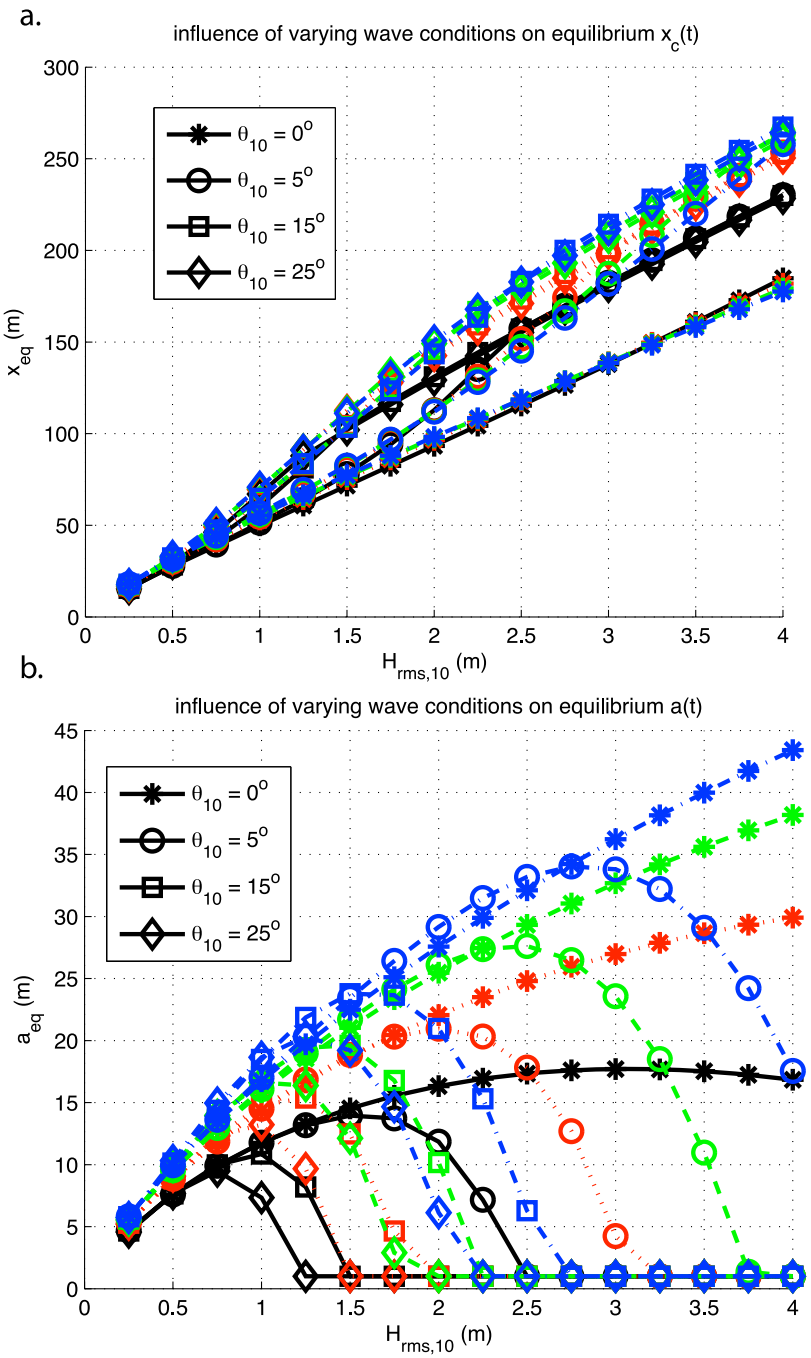

Figure 13. Equilibrium analysis for varying wave conditions, using the dynamically coupled 2DH model. T = 6 s (black solid), T = 8 s (red dotted), T = 10 s (green dashed), and T = 12 s (blue dash-dotted). Symbols represent different θ_{10} values.

assumption that the dominant mode of nearshore variability is the migration of roughly constant form sandbars. Model equations describing the temporal evolution of sandbar position and sandbar 2DH variability are derived based on an equilibrium approach and include parametric drivers. The model is tested on 566 days of data, covering a large range of forcing conditions, as well as onshore and offshore migration events. The dynamic model is capable of predicting bar position and 2DH variability with significant skill over multiple storm events given incident wave forcing

Table 7. Calibration Coefficients and Model Skill Based on Best Fit to Individual Data Sets for Dynamically Coupled Model

Data Set	α_1	α_2	α_3	α_4	$R_{x\hat{x}}^2$	$R_{a\hat{a}}^2$
April 1996	3.44	0.11	7.78	0.04	0.91	0.91
July 1996	1.23	0.06	2.58	0.03	0.27	0.17
May 1997	2.61	0.09	0.68	0.01	0.87	0.77
October 1997	1.36	0.14	1.14	0.04	0.80	0.24
March 1998	2.12	0.21	1.30	0.03	0.76	0.71
May 1998	2.73	0.07	1.21	0.03	0.70	0.59
April 1999	0.76	0.06	10.70	0.04	0.46	0

($R_{x\hat{x}}^2$ = 0.49, $R_{a\hat{a}}^2$ = 0.41). Spectral comparisons of measured versus modeled bar position and 2DH variability were significantly coherent for periods longer than 9 days. To our knowledge, this is the first model to reasonably predict short-term bar response for multistorm timescales.

[50] The model contains two pieces of physics not previously considered important in describing sandbar migration. First, sediment transport is nonlinearly dependent on the presence of wave breaking over the bar. In the absence of breaking, no migration is assumed to occur, agreeing well with observations of breaking patterns (sandbars) from video images. The inclusion of such a term also accounts for the observed stranding of offshore storm bars under prolonged calm wave periods and limits sediment transport under mild wave conditions as compared to previous linear equilibrium-based parametric models [e.g., *Plant et al.*, 2006]. Second, the model explicitly includes the influence of 2DH morphology on alongshore-averaged sandbar migration rates. The inclusion of a term describing the influence of 2DH processes, modeled here as κ_a, was important in predicting onshore migration rates under intermediate wave breaking. Compared to a 1DH version of the model, the inclusion of 2DH terms showed large improvement in model skill (1DH Brier skill score = −0.12 versus 0.42 for 2DH). The 1DH model was biased toward offshore sandbar migration and was unable to reproduce the measured onshore migration rates. The inclusion of κ_a coupling bar migration to 2DH morphologic evolution in the equilibrium balance shifted transport to onshore migration under intermediate wave breaking and prevented the bar from moving offshore under intermediate waves when 2DH morphology was significant. This agrees well with observations of onshore sandbar migration in the presence of 2DH morphology and increased stability of 2DH systems against larger waves by reducing undertow in favor of circulation (hysteresis). The results presented here suggest that both variations in the amount of wave breaking present over the sandbar and the underlying amount of 2DH morphology influence sandbar migration rates and stability of the system and warrant further study.

Appendix A: Formulation of ζ

[51] It has been commonly observed that the effect of alongshore-variable forcing or morphology becomes muted [e.g., *Yu and Slinn*, 2003] in the presence of strong alongshore currents, so the dependence on 2DH morphology should be reduced. *Wilson* [2009] examined the effects of alongshore nonuniform dynamics in the surf zone using the steady state, depth-integrated and wave-averaged equations of motion [*Mei*, 1989]. Neglecting the effects of wind and momentum mixing, it has been shown that the cross-shore wave forcing due to radiation stress gradients is roughly balanced by the cross-shore pressure gradient and thus the relationship between the alongshore component of wave forcing due to radiation stress gradients and the alongshore pressure gradient are a function of the alongshore variable wave forcing, $F(x,y)$. They partitioned the bathymetry and wave forcing into alongshore-uniform and alongshore-variable components, $h_o(x)$ and $h_1(x,y)$, $F_0(x)$ and $F_1(x)e^{ik_y y}$, respectively, and the forced longshore current into corresponding steady and variable components, $v_0(x)$ and $v_1(x,y)$. Assuming cross-shore advection terms were relatively unimportant, and neglecting higher-order terms, they arrived at

$$\rho_w h_o v_o \frac{\partial v_1}{\partial y} = F_o + F_1 e^{ik_y y} - \rho_w c_f u_w (v_o + v_1), \tag{A1}$$

where c_f is the wave friction factor, taken to be 0.01, k_y, is the alongshore wave number of variability, and u_w is the wave orbital velocity. Separating the alongshore variable component

$$\rho_w h_o v_o \frac{\partial v_1}{\partial y} = F_1 e^{ik_y y} - \rho_w c_f u_w v_1, \tag{A2}$$

that has the solution (taking the real part)

$$\begin{aligned} v_1 &= \Re\left\{\frac{F_1}{\rho_w c_f u_w}[1 + iRe_s]^{-1} e^{ik_y y}\right\} \\ &= \zeta \frac{F_1}{\rho_w c_f u_w} \sin\left[k_y y + \sin^{-1}\zeta\right]. \end{aligned} \tag{A3}$$

This states that both the attenuation and phase shift of v_1 depend only on the nondimensional parameter, ζ:

$$\zeta = \frac{1}{\sqrt{1 + Re_s^2}}, \tag{A4}$$

which in turn, depends only on the "shallow water Reynolds number" [*Allen et al.*, 1996]:

$$Re_s = \frac{k_y h_o v_o}{c_f u_w}, \tag{A5}$$

or the ratio of the frictional timescale ($h_o/c_f\ u_w$) to the advective timescale $(k_y\ v_o)^{-1}$. Replacing h_o with the depth at the bar crest, h_{x_c}, and approximating the alongshore current using $v_o = 2.7\ u_w \sin\theta\cos\theta$ [*Komar and Inman*, 1970], Re_s can be simplified to

$$Re_s = \frac{2.7}{c_f} k_y h_{x_c} \sin\theta\cos\theta. \tag{A6}$$

Equation (A6) states that as the wave angle increases, the effect of alongshore variability is damped out, reducing v_1 and by continuity, u_1, the alongshore-variable component of the cross-shore current. If we take $k_y = 2\pi/L_y$ to be the representative wave number of alongshore variability of the bar (for Palm Beach, we have chosen a static alongshore length scale of L_y = 150 m), this formulation suggests wave angles greater than roughly 5 degrees at the breakpoint reduce the effects of 2DH morphology by 50%.

Notation

$a(t)$,$\hat{a}(t)$	measured and modeled 2DH variability of the sandbar, respectively, m.
a_o	reference 2DH variability, for Palm Beach, a_o = 15 m, m.
α_1–α_4	nondimensional free parameters in model.
$b(t)$	fraction of breaking waves
β	beach slope, for Palm Beach, β = 0.029.
B	relative bias.

BSS Brier skill score.
c wave celerity, m s^{-1}.
C_d drag coefficient, constant 0.003.
c_f Wave friction factor, constant 0.01.
d_{50} median grain size, for Palm Beach, d_{50} = 0.3 mm, mm.
δ_{tide} tidal range, for Palm Beach, δ_{tide} = 1 m, m.
$\Delta_{x_c}(t)$ height of bar measured at bar crest location, x_c, m.
Δ_o reference bar height measured at reference location, x_o, m.
ϵ_s suspended load efficiency factor, constant 0.015.
$f_{\Delta x_c}, f_{Lx_c}$ cross-shore bar height and length dependencies, respectively.
G growth/decay term describing changes in a.
$\gamma_b(t)$ breaking relative wave height, H_b/h_{x_c}.
γ_{eq} equilibrium relative wave height, set to 0.65.
$\gamma_{x_c}(t)$ relative wave height at bar crest, H_{x_c}/h_{x_c}.
$h(x, y, t)$ water depth, m.
$h_{x_c}(t)$ depth at bar crest location, defined as $h_{x_c} = \beta x_c - \Delta_{x_c}$, m.
$H_b(t)$ breaking wave height, m.
$H_{x_c}(t)$ wave height modeled at bar crest, m.
$H_{\mathrm{RMS},o}(t)$ offshore root mean square wave height, m.
$H_{\mathrm{RMS},10}(t)$ root-mean-square wave height, modeled at 10 m depth, m.
k_y alongshore wave number of sandbar, set here to 0.04 for Palm Beach, m^{-1}.
K_s dimensionless suspended load transport coefficient.
$\kappa_a(t)$ relative influence factor of 2DH processes on cross-shore sediment transport.
m coefficient in cross-shore bar length formulation, constant 0.27.
M magnitude of bar migration at bar crest, m d^{-1}.
μ sediment packing factor, constant 0.65.
Ω nondimensional fall velocity, $\Omega = H_b/TW$.
$Q_x(x,t)$ cross-shore volumetric sediment transport per unit width, m^2 d^{-1}.
$Q_{x_{xc}}(t)$ total cross-shore transport modeled at bar crest, m^2 d^{-1}.
$\hat{Q}_{x_{xc}}(t)$ magnitude of cross-shore transport modeled at bar crest, m^2 d^{-1}.
RMSE root-mean-square error.
R^2 squared correlation coefficient.
Re_s shallow water Reynolds number.
T wave period, s.
T_o reference wave period, set here to mean value for Palm Beach of 10 s, s
$\theta(t)$ wave angle with respect to shore normal, deg.
$\theta_{x_c}(t)$ wave angle with respect to shore-normal modeled at bar crest, deg.
$\theta_{10}(t)$ wave angle with respect to shore-normal modeled at 10 m depth, deg.
$u(t),U(t),u_w(t)$ total velocity, depth-averaged cross-shore current, and wave orbital velocity, respectively, m s^{-1}.
$U_s(t),U_r(t)$ return flow due to Stokes drift and roller, respectively, m s^{-1}.
w weighting factor used to describe quality of image data.
W sediment fall velocity, set to 0.04 m s^{-1}, m s^{-1}.
$x_{bar}(y,t)$ video-derived sandbar position, m.
$x_c(t),\hat{x}_c(t)$ measured and modeled alongshore-averaged sandbar crest position, m s^{-1}.
x_o reference location where Δ_o is measured, m.
$x_s(y,t)$ video-derived shoreline position, m.
$\zeta(t)$ relative influence of wave angle and morphology on 2DH currents.

[52] **Acknowledgments.** This research was made possible with the help and data provided by many people. T. Lippmann provided cross-shore wave heights, profiles, and wave breaking data from Duck94. Daily RMS wave heights and angles for Palm Beach were provided by G. Symonds. The authors also extend their appreciation to J. Stanley for always knowing where the data are and for his unending patience and technical savvy for all things Argus database related; H. T. Özkan-Haller, J. Long, M. Palmsten, and G. Wilson for their insight into the problem; and A. Bowen, an eternal mentor. The authors also extend their sincere appreciation to the reviewers of this manuscript whose extensive comments greatly improved the quality of this paper. This research was generously funded by ONR SECNAV/CNO Chair of Oceanography (N00014-03-1-0973) and the Coastal Geosciences Program (N00014-07-1-0490).

References

Alexander, P. S., and R. A. Holman (2004), Quantitative analysis of nearshore morphological variability based on video imaging, *Mar. Geol.*, *208*(1), 101–111.

Allen, J. S., P. A. Newberger, and R. A. Holman (1996), Nonlinear shear instabilities of alongshore currents on plane beaches, *J. Fluid Mech.*, *310*, 181–213.

Bagnold, R. A. (1941), *The Physics of Blown Sand and Desert Dunes*, Methuen, New York.

Bagnold, R. A. (1963), Mechanics of marine sedimentation, in *The Sea*, vol. 3, edited by M. Hill, pp. 507–528, Wiley-Interscience, New York.

Bailard, J. A. (1981), An energetics total load sediment transport model for a plane sloping beach, *J. Geophys. Res.*, *86*(C11), 10,938–10,954.

Bowen, A. J. (1980), Simple models of nearshore sedimentation; beach profiles and longshore bars, in *The Coastline of Canada*, vol. Paper 80-10, edited by S. McCann, pp. 1–11, Geological Survey of Canada, Ottawa.

Calvete, D., N. Dodd, A. Falques, and S. van Leeuwen (2005), Morphological development of rip channel systems: Normal and near normal wave incidence, *J. Geophys. Res.*, *110*, C10006, doi:10.1029/2004JC002803.

Coco, G., and A. B. Murray (2007), Patterns in the sand: From forcing templates to self-organization, *Geomorphology*, *91*, 271–290.

Dean, R. G., and R. A. Dalrymple (1991), *Water Wave Mechanics for Engineers and Scientists*, vol. 2, World Sci., Singapore.

Drønen, N., and R. Deigaard (2007), Quasi-3-D modelling of the morphology of longshore bars, *Coastal Eng.*, *54*, 197–215.

Durran, D. R. (1999), *Numerical Methods for Wave Equations in Geophysical Fluid Dynamics*, Springer, New York.

Elgar, S., E. L. Gallagher, and R. Guza (2001), Nearshore sandbar migration, *J. Geophys. Res.*, *106*, 11,623–11,627.

Feddersen, F., and R. T. Guza (2003), Observations of nearshore circulation: Alongshore uniformity, *J. Geophys. Res.*, *108*(C1), 3006, doi:10.1029/2001JC001293.

Gallagher, E. L., R. T. Guza, and S. Elgar (1998), Observations of sand bar evolution on a natural beach, *J. Geophys. Res.*, *103*(C2), 3203–3215.

Garnier, R., D. Calvete, A. Falques, and N. Dodd (2008), Modelling the formation and the long-term behavior of rip channel systems from the deformation of a longshore bar, *J. Geophys. Res.*, *113*, C07053, doi:10.1029/2007JC004632.

Haller, M. C., R. A. Dalrymple, and I. A. Svendsen (2002), Experimental study of nearshore dynamics on a barred beach with rip channels, *J. Geophys. Res.*, *107*(C6), 3061, doi:10.1029/2001JC000955.

Henderson, S. M., J. S. Allen, and P. A. Newberger (2004), Nearshore sandbar migration predicted by an eddy-diffusive boundary layer model, *J. Geophys. Res.*, *109*, C06024, doi:10.1029/2003JC002137.

Hoefel, F., and S. Elgar (2003), Wave-induced sediment transport and sandbar migration, *Science*, *299*(5614), 1885–1887.

Holland, K. T., R. A. Holman, T. C. Lippmann, J. Stanley, and N. G. Plant (1997), Practical use of video imagery in nearshore oceanographic field studies, *IEEE J. Ocean Eng.*, *22*(1), 81–92, doi:10.1109/48.557542.

Holman, R. A., J. Stanley, and H. T. Özkan Haller (2003), Applying video sensor networks to nearshore environmental monitoring, *IEEE Pervasive Comput.*, *2*(4), 14–21.

Holman, R. A., G. Symonds, E. B. Thornton, and R. Ranasinghe (2006), Rip spacing and persistence on an embayed beach, *J. Geophys. Res.*, *111*, C01006, doi:10.1029/2005JC002965.

Holthuijsen, L. H., N. Booij, and T. H. C. Herbers (1989), A prediction model for stationary, short-crested waves in shallow water with ambient currents, *Coastal Eng.*, *17*(23), 211–225.

Komar, P. D. (1974), *Beach Processes and Sedimentation*, Prentice-Hall, Englewood Cliffs, N. J.

Komar, P. D., and D. L. Inman (1970), Longshore sand transport on beaches, *J. Geophys. Res.*, *75*, 5914–5927.

Kriebel, D. L., and R. G. Dean (1985), Numerical simulation of time-dependent beach and dune erosion, *Coastal Eng.*, *9*, 221–245.

Larson, M., and N. C. Kraus (1989), Sbeach: Numerical model for simulating storm-induced beach change; report 1, empirical foundation and model development, *Tech. Rep. 89-9*, *Coastal Eng. Res. Cent.*, U.S. Army Eng. Waterw. Exp. Stn., Vicksburg, Miss.

Lippmann, T. C., and R. A. Holman (1989), Quantification of sand bar morphology: A video technique based on wave dissipation, *J. Geophys. Res.*, *94*(C1), 995–1011.

Lippmann, T. C., and R. A. Holman (1990), The spatial and temporal variability of sand bar morphology, *J. Geophys. Res.*, *95*(C7), 11,575–11,590.

Mei, C. C. (1989), *The Applied Dynamics of Ocean Surface Waves*, World Sci., Singapore.

Pape, L., B. G. Ruessink, M. A. Wiering, and I. L. Turner (2007), Recurrent neural network modeling of nearshore sandbar behavior, *Neural Networks*, *20*, 509–518, doi:10.1016/j.neunet.2007.04.007.

Pape, L., Y. Kuriyama, and B. G. Ruessink (2010a), Models and scales for cross-shore sandbar migration, *J. Geophys. Res.*, *115*, F03043, doi:10.1029/2009JF001644.

Pape, L., N. G. Plant, and B. G. Ruessink (2010b), On cross-shore migration and equilibrium states of nearshore sandbars, *J. Geophys. Res.*, *115*, F03008, doi:10.1029/2009JF001501.

Plant, N. G., R. A. Holman, and M. H. Freilich (1999), A simple model for interannual sand bar behavior, *J. Geophys. Res.*, *104*(C7), 15,755–15,776.

Plant, N. G., M. H. Freilich, and R. A. Holman (2001), The role of morphological feedback in surf zone sand bar response, *J. Geophys. Res.*, *106*(C1), 973–989.

Plant, N. G., K. Todd Holland, and R. A. Holman (2006), A dynamical attractor governs beach response to storms, *Geophys. Res. Lett.*, *33*, L17607, doi:10.1029/2006GL027105.

Ranasinghe, R., G. Symonds, K. Black, and R. A. Holman (2004), Morphodynamics of intermediate beaches: a video imaging and numerical modeling study, *Coastal Eng.*, *51*, 629–655.

Reniers, A. J. H. M., J. A. Roelvink, and E. B. Thornton (2004), Morphodynamic modeling of an embayed beach under wave group forcing, *J. Geophys. Res.*, *109*, C01030, doi:10.1029/2002JC001586.

Roelvink, J. A., and M. J. F. Stive (1989), Bar-generating cross-shore flow mechanisms on a beach, *J. Geophys. Res.*, *94*(C4), 4785–4800.

Ruessink, B. G., J. R. Miles, F. Feddersen, R. T. Guza, and S. Elgar (2001), Modeling the alongshore current on barred beaches, *J. Geophys. Res.*, *106*(C10), 22,451–22,463.

Ruessink, B. G., K. M. Wijnberg, R. A. Holman, Y. Kuriyama, and I. M. J. van Enckevort (2003), Intersite comparison of interannual nearshore bar behavior, *J. Geophys. Res.*, *108*(C8), 3249, doi:10.1029/2002JC001505.

Ruessink, B. G., Y. Kuriyama, A. J. H. M. Reniers, J. A. Roelvink, and D. J. R. Walstra (2007), Modeling cross-shore sandbar behavior on the timescale of weeks, *J. Geophys. Res.*, *112*, F03010, doi:10.1029/2006JF000730.

Sallenger, A. H., Jr., and P. A. Howd (1989), Nearshore bars and the breakpoint hypothesis, *Coastal Eng.*, *12*, 301–313.

Short, A. D., and N. L. Trenaman (1992), Wave climate of the Sydney region, and energetic and highly variable ocean wave regime, *Aust. J. Mar. Freshwater Res.*, *43*, 765–791.

Splinter, K. D. (2009), Development of 2D models to estimate nearshore bathymetry and sediment transport, Ph.D. thesis, Oreg. State Univ., Corvallis.

Svendsen, I. A. (1984), Mass flux and undertow in a surf zone, *Coastal Eng.*, *8*, 347–364.

Thornton, E. B., and R. T. Guza (1983), Transformation of wave height distribution, *J. Geophys. Res.*, *88*(C10), 5925–5938.

van Enckevort, I. M. J., B. G. Ruessink, G. Coco, K. Suzuki, I. L. Turner, N. G. Plant, and R. A. Holman (2004), Observations of nearshore crescentic sandbars, *J. Geophys. Res.*, *109*, C06028, doi:10.1029/2003JC002214.

Wilson, G. W. (2009), Field validation of a nearshore circulation model for alongshore-nonuniform flows, Master's thesis, Oreg. State Univ., Corvallis.

Wright, L. D., and A. D. Short (1984), Morphodynamic variability of surf zones and beaches: A synthesis, *Mar. Geol.*, *56*, 93–118.

Wright, L. D., F. C. Coffey, and P. J. Cowell (1980), Nearshore oceanography and morphodynamics of the Broken Bay - Palm Beach region, N.S.W.: Implications for offshore dredging, *Tech. Rep. 80/1*, *Coastal Stud. Unit*, Dep. of Geogr.,Univ. of Sydney, Sydney, Australia.

Wright, L. D., A. D. Short, and M. O. Green (1985), Short-term changes in the morphodynamic states of beaches and surf zones: An empirical predictive model, *Mar. Geol.*, *62*, 339–364.

Wright, L. D., A. D. Short, J. D. Boon III, B. Hayden, S. Kimball, and J. H. List (1987), The morphodynamic effects of incident wave groupiness and tide range on an energetic beach, *Mar. Geol.*, *74*, 1–20.

Yu, J., and D. N. Slinn (2003), Effects of wave-current interaction on rip currents, *J. Geophys. Res.*, *108*(C3), 3088, doi:10.1029/2001JC001105.

R. A. Holman, College of Oceanic and Atmospheric Sciences, Oregon State University, 104 Ocean Admin Bldg., Corvallis, OR 97331, USA. (holman@coas.oregonstate.edu)

N. G. Plant, U.S. Geological Survey, Florida Integrated Science Center, 600 Fourth St. South, St. Petersburg, FL 33701, USA. (nplant@usgs.gov)

K. D. Splinter, Griffith Centre for Coastal Management, Griffith University, Gold Coast Campus, Southport, QLD 4222, Australia. (k.splinter@griffith.edu.au)